Nanoscale

Biocompatible Triboelectric Energy Generators (BT-TENGs) for Energy Harvesting and Healthcare Applications

Journal:	*Nanoscale*
Manuscript ID	NR-REV-05-2024-001987.R1
Article Type:	Review Article
Date Submitted by the Author:	20-Aug-2024
Complete List of Authors:	Ramaraj, Sankar Ganesh; The University of Tokyo, Bioengineering E, Durgadevi; Roever Engineering College Tabata, Hitoshi; University of Tokyo, Department of Bioengineering Zhang, Fuchun; Yan'an University, Liu, Xinghui; Sungkyunkwan University, Chemistry;

Biocompatible Triboelectric Energy Generators (BT-TENGs) for Energy Harvesting and Healthcare Applications

Sankar Ganesh Ramaraj [a, b, e, *], Durgadevi Elamaran [c, *], Hitoshi Tabata [b, d], Fuchun zhang [a], Xinghui Liu [f, g, h *]

[a] School of Physics and Electronic Information, Yan'an University, Yan'an, 716000, China

[b] Department of Bioengineering, The University of Tokyo, 7-3-1 Hongo, Bunkyo-Ku, Tokyo 113-8656, Japan.

[c] Graduate School of Arts and Sciences College of Arts and Sciences, The University of Tokyo, Komaba Campus, Tokyo, Japan.

[d] Department of Electrical Engineering and Information Systems, Graduate School of Engineering, The University of Tokyo, 7-3-1 Hongo, Bunkyo-ku, Tokyo 113-8656, Japan

[e] Department of Materials Physics, Saveetha School of Engineering, Saveetha Institute of Medical and Technical Sciences (SIMTS), Thandalam, Chennai -602105, Tamilnadu, India.

[f] Science and Technology on Aerospace Chemical Power Laboratory, Laboratory of Emergency Safety and Rescue Technology, Hubei Institute of Aerospace Chemotechnology, Xiangyang 441003, China.

[g] Division of Research and Development, Lovely Professional University, Phagwara, India

[h] College of Chemistry and Molecular Engineering, Peking University, Beijing, 100871, China; Graphene Basic Science Research Center, Beijing Graphene Institute (BGI), Beijing, 100095, China.

Corresponding authors: Sankar Ganesh Ramaraj ramaraj@g.ecc.u-tokyo.ac.jp; Durgadevi Elamaran durgaelamaran@gmail.com; Xinghui Liu: liuxinghui119@gmail.com

Abstract

Electronic waste (e-waste) has become a significant environmental and societal challenge, necessitating the development of sustainable alternatives. Biocompatible and biodegradable electronic devices offer a promising solution to mitigate e-waste and provide viable alternatives for various applications, including triboelectric nanogenerators (TENGs). This review provides a comprehensive overview of recent advancements in biocompatible, biodegradable, and implantable TENGs, emphasizing their potential as energy scavengers for healthcare devices. The review delves into the fabrication processes of self-powered TENGs using natural biopolymers, highlighting their biodegradability and compatibility with biological tissues. It further explores the biomedical applications of ultrasound-based TENGs, including

their roles in wound healing and energy generation. Notably, the review presents the novel application of TENGs for vagus nerve stimulation, demonstrating their potential in neurotherapeutic interventions. Key findings include the identification of optimal biopolymer materials for TENG fabrication, the effectiveness of TENGs in energy harvesting from physiological movements, and the potential of these devices in regenerative medicine. Finally, the review discusses the challenges in scaling up the production of implantable TENGs from biomaterials, addressing issues such as mechanical stability, long-term biocompatibility, and integration with existing medical devices, outlining future research opportunities to enhance their performance and broaden their applications in the biomedical field.

Keywords Biocompatible, biodegradable, ultrasound, nerve stimulator, Implantable triboelectric nanogenerator

1. Introduction

In recent years, the development of smart wearable electronic devices has experienced a notable surge, fueled by their versatile applications across healthcare systems, communication devices, and energy storage solutions [1–5]. However, a significant challenge hindering their advancement revolves around sourcing sustainable power. Commercial batteries, while commonly used, pose drawbacks such as weight, lengthy recharging times, and limited lifespans, making them less suitable for the demands of smart wearable electronics. Additionally, the reliance on conventional batteries contributes to the growing issue of electronic waste (e-waste). E-waste is one of the fastest-growing waste streams globally, with millions of tons generated each year. This waste often ends up in landfills or is improperly disposed of, leading to the release of hazardous substances like lead, mercury, and cadmium into the environment [4]. These toxic materials can contaminate soil and water sources, posing severe risks to ecosystems and human health. Moreover, the extraction of raw materials for battery production, such as lithium and cobalt, further exacerbates environmental degradation, often involving harmful mining practices that contribute to deforestation, soil erosion, and loss of biodiversity. The environmental impact of e-waste is compounded by the fact that many wearable devices have short life cycles, driven by rapid technological advancements and

consumer demand for the latest features [5]. As a result, these devices are frequently discarded, adding to the growing e-waste problem. The disposal and recycling of electronic components are often inefficient, with only a small percentage of e-waste being properly recycled [6, 7]. This inefficiency underscores the urgent need for the development of sustainable, eco-friendly alternatives that not only provide reliable power for wearable electronics but also reduce the overall environmental footprint of these devices. In light of these challenges, there is a growing emphasis on researching and developing energy harvesting technologies, such as triboelectric nanogenerators (TENGs), which can convert biomechanical energy from daily human activities into electrical power. These technologies have the potential to offer a more sustainable and environmentally friendly solution, reducing reliance on traditional batteries and mitigating the negative impacts associated with e-waste [6-8]. Meanwhile, human skin serves as a pivotal interface between the body and the external environment, endowed with remarkable sensory capabilities facilitating perception, interaction, and communication with surroundings. This intrinsic functionality has spurred a surge of interest in bioinspired electronic skins (e-skins) [9]. These e-skins emulate the multifaceted characteristics of natural skin and find applications spanning wearable health monitoring, prosthetics, robotics, human-machine interfaces, and artificial intelligence [10-11]. Addressing this challenge requires tapping into ubiquitous mechanical energy sources like vibrations, body movements, wind, and hydro energy [9-10]. Biomechanical energy, derived from human body movements, holds significant potential for powering wearable electronics, human-machine interactions, and biomedical devices [11-13]. While capacitive and piezoelectric sensors have shown promise in real-time health monitoring, their reliance on external power sources adds complexity and energy consumption to wearable devices [14-16]. Enter the triboelectric nanogenerator (TENG), introduced in 2012 as a game-changer in energy harvesting. TENG-based devices offer a cost-effective solution, enabling the fabrication of miniature, portable energy harvesters and self-powered sensors [17-20]. Operating on the principle of electron affinity generated by friction between different materials, TENGs prioritize the selection of triboelectric materials. However, conventional materials like metal, poly(tetrafluoroethylene) (PTFE), and copper pose environmental challenges due to their non-renewable nature, lack of biodegradability, and cost [21-25]. As sustainability becomes increasingly critical, the quest for biodegradable, biocompatible, lightweight, and cost-effective materials gains momentum. This pursuit is not only driven by environmental concerns but also

by the rise of electronic waste (e-waste) and the need for implantable devices that minimize environmental impact [26-33]. In the realm of biomedical devices, implantable technologies have garnered significant attention for their potential to enhance human life expectancy and facilitate real-time health monitoring. Implantable TENGs have found application in diverse medical equipment, including Electrocardiography (ECGs), cochlear prostheses, pacemakers, and brain and nerve stimulators, among others [33-37]. However, challenges persist in terms of fabrication, size, cost, and weight, underscoring the importance of using biocompatible and biodegradable materials to enhance comfort and efficacy in daily health monitoring [38-40]. In addition, However, there are instances where electronic implants are only required for a specific duration, aligned with a transient biological process like wound healing. In such cases, the utilization of bioresorbable materials enables the development of devices that naturally dissolve into the body after fulfilling their operational timeframe. Previous studies have demonstrated that water-soluble materials, such as monocrystalline silicon (Si), metals (Mg, Mo, Fe, Zn, and W), metal oxides (SiO2, MgO, and Si3N4), and organic polymers (silk fibroin and collagen), can form the foundation for various active and passive bioresorbable components, including transistors, capacitors, resistors, and diodes [9-10].

This review focuses on and summarises the biocompatible and biodegradable implantable TENG applications (figure 1). In addition, Ultrasound-based triboelectric generators in the field of health analysis and power generation are then discussed. Finally, the use of TENGs for neurostimulation is discussed.

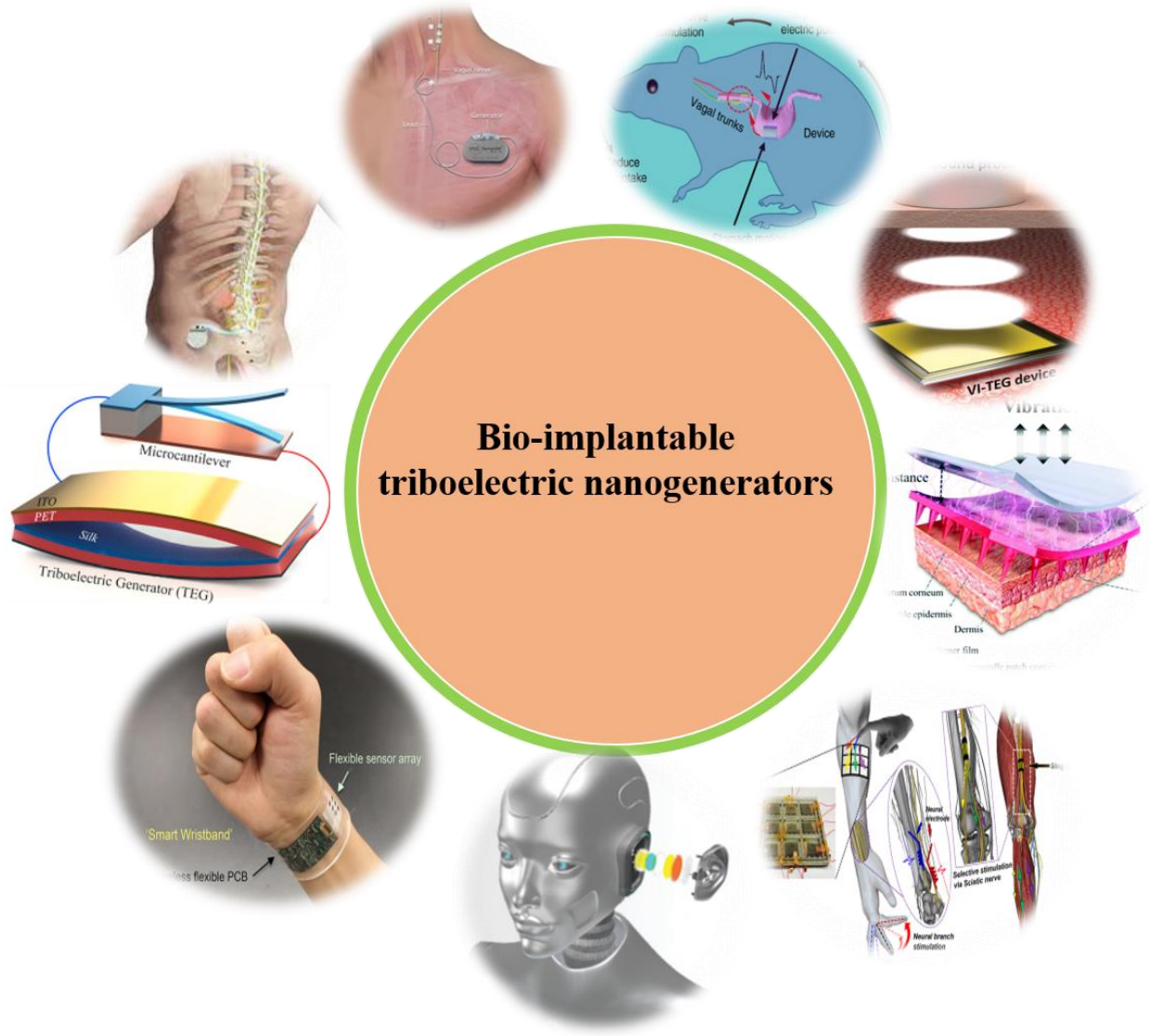

Figure 1 Schematic illustration of bio-implantable triboelectric nanogenerator

2. Different types Triboelectric nanogenerators

TENGs operate on the coupling effects of contact electrification and electrostatic induction. When two different materials with reverse polarity come into are in contact, the electrification induction effect occurs, which in turn causes the flow of charges in the electrodes. TENGs operate on four principles, namely, vertical contact-separation (C-S), single-electrode, lateral sliding, and free-standing modes as shown in Figure 2 [41-45].

2.1 Vertical C-S mode

The vertical C-S TENG is one of the primary innovations among the four TENG operating modes. The device consists of two different triboelectric materials attached to

electrodes on the backside of the surface. When these materials come into contact with each other due to an external force, surface charge variation is created owing to the electrification effect. When the applied pressure is released, the materials are separated and a potential is formed, driving charges from one electrode to another to maintain the electrical potential equilibrium owing to electrostatic induction. This leads to the creation of an alternate current. When the force is applied again, the charges flow back to their original electrode, inducing a temporary alternating current (AC) to flow in the reverse direction. The main advantage of the vertical C-S mode is that it can be utilised in biomedical applications owing to its low operating frequency [46-47].

2.2 Lateral sliding Mode

The structure employed for lateral sliding TENGs is similar to that of the vertical C-S TENG; however, triboelectric charges are generated by the lateral sliding of the two friction layers. Electrons flow through the electrodes when the friction material slides and contacts with each other. Lateral sliding TENGs possess a higher charge efficiency than the C-S TENGs. However, lateral sliding TENGs exhibit poor durability and stability [48-51].

2.3 Single-electrode mode

The working principle and structure of the single-electrode-mode TENG are different from those of the aforementioned methods. The single-electrode mode consists of only one friction layer with a single grounded electrode. This TENG uses moving objects as a second frictional layer that operates directly on it. However, the output obtained from this type of TENG is relatively low, as compared to that of the other methods [52,53].

2.4 Free-standing mode

In free-standing TENGs, the dielectric layer moves freely on the surface of two fixed metal electrodes. The movement of the dielectric material between the friction materials leads to an asymmetric charge distribution, which in turn generates electron flow in the circuit. Free-standing TENGs can achieve higher power conversion and durability than the other types of TENGS. This property facilitates the use of free-standing TENG devices in energy harvesting applications [54-55].

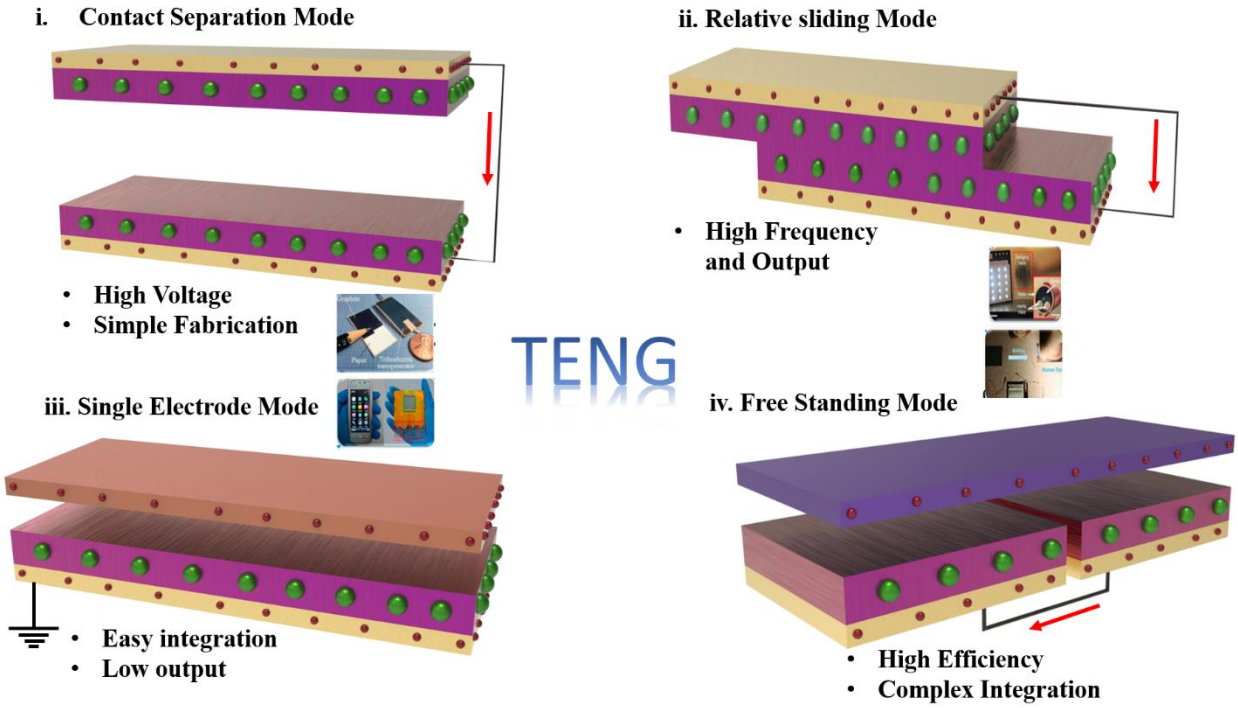

Figure. 2 Schematic representation of different modes of triboelectric nanogenerators.

The theoretical mechanism of a TENG can be elucidated using Gauss's theorem, which captures the interrelation among voltage, charge, and motion (V–Q–x) over time. In this context, the two triboelectric materials, D1 and D2, possess thicknesses of d_1 and d_2 with relative permittivity's ε_{r1} and ε_{r2}, respectively. Under a periodic external force, the separation distance xxx varies over time. When D1 and D2 come into contact due to the applied force, opposite static charges with a surface charge density σ_{sc} are generated on their inner surfaces. Upon the release of the external force, the materials separate, creating a potential difference (V) between the electrodes. The charge transfers between the electrodes M1 and M2, denoted as Q (i.e., −Q on M1 and Q on M2), is determined. Using Gauss's theorem, the voltage difference across D1, D2, and the air gap can be expressed, reflecting the complete process [56].

$$V(t)=E_1d_1+E_2d_2+E_{air}x \quad (1)$$

The relationships of V-Q-x are then described by substituting $\boldsymbol{\sigma_{sc}}$ into the eq 1 as shown below

$$V(t) = -\frac{Q}{S_{\varepsilon 0}}\left(\frac{d_1}{\varepsilon_{r1}} + \frac{d_2}{\varepsilon_{r2}} + x(t)\right) + \frac{\sigma_{sc}}{\varepsilon_0}x(t) \quad (2)$$

From Eq. 2, under open-circuit conditions, the charges on the electrode remain stationary, resulting in zero current. Consequently, the open-circuit voltage (Voc) can be derived as follows:

$$V_{oc}(t) = \frac{\sigma_{sc}}{\varepsilon_0} x(t) \quad (3)$$

In addition, under the short circuit conditions, the voltage potential difference drops to zero (V(t)=0). The resulting transfer of charges Q_{sc} and the short-circuit current I_{sc} can be expressed as

$$Q_{sc}=\left[\frac{S_{\sigma_{sc}} x(t)}{\left(\frac{d_1}{\varepsilon_{r1}}+\frac{d_2}{\varepsilon_{r2}}+x(t)\right)}\right] \quad (4)$$

$$I_{sc}=\frac{dQ_{sc}}{dt} = \frac{d}{dt}\left[\frac{S_{\sigma_{sc}} x(t)}{\left(\frac{d_1}{\varepsilon_{r1}}+\frac{d_2}{\varepsilon_{r2}}+x(t)\right)}\right] = \frac{S_{\sigma_{sc}}\left(\frac{d_1}{\varepsilon_{r1}}+\frac{d_2}{\varepsilon_{r2}}\right)V(t)}{\left(\frac{d_1}{\varepsilon_{r1}}+\frac{d_2}{\varepsilon_{r2}}+x(t)\right)^2} \quad (5)$$

To better understand the working mechanism of TENGs, we present Maxwell's displacement current and the expanded form of Maxwell's equations. These fundamental equations, a set of partial differential equations, describe fluctuations in electromagnetic fields, where waves propagate at a constant speed ccc (approximately 3×10^8 m/s in a vacuum), as shown below:

Gauss's law $\nabla \times D'$ (6)

$$\nabla \times B = 0 \quad (7)$$

Gauss's law correlated to magnetism

Faraday law $\nabla \times E = \frac{\partial B}{\partial t}$ (8)

Ampere- Maxwell law $\nabla \times H = J_f + \frac{\partial D'}{\partial t}$ (9)

where D is the displacement field, ρ_f is the free electric charge density, B is the magnetic field, E is the electric field, H is the magnetizing field, J_f is the free electric current density.

The differential form of Maxwell's equations, as presented above, applies to systems with fixed boundaries and volumes of dielectric media, making them time-independent. In this context, electromagnetic waves are generated and propagated in stationary media. However, significant challenges arise when dealing with systems involving moving charged media and time-dependent configurations [56].

3. Biocompatible and Biodegradable TENGs as energy harvesters

A new class of electronic materials with crucial properties, such as ultra-stretchability, softness, toughness, self-healing, biocompatibility, and biodegradability, is necessary for next-generation electronic devices [57-58]. Researchers and industry have recently focused on the biocompatibility and biodegradability of energy-harvesting devices because of the significant

amount of e-waste that is becoming a major threat to the ecological system [59]. Moreover, a recent analysis estimated that 53.6 million tons of e-waste has been produced globally and it is estimated that 74.7 million tons of e-waste will be produced by 2030 [60, 61]. Therefore, biocompatible and biodegradable materials are required to address this problem. However, the discovery and fabrication of biodegradable materials remains challenging.

3.1 Cellulose-based TENGs

Cellulose is an organic polymer available in most plants, and certain microbes, such as *Acetobacter xylinum*, can biosynthesise it. The glycosyl group of cellulose has a large number of hydroxyl groups, which can build a large number of hydrogen bonds, generating a robust hydrogen bonding network [62-63]. Because of their distinct structures and chemical properties, nanocellulose and cellulose derivatives may be produced using various physical and chemical processes using cellulose as the raw material, increasing the availability of cellulose-based goods. Consequently, they are widely employed in everyday life, such as in papermaking, coating, textiles, everyday chemicals, health care items, and pharmaceuticals [65,66]. Hence, researchers have begun working on these materials. For example, Lamanna *et al.* [67] used drop-casting to fabricate cellulose-based edible TENGs (CETNs), and different edible films were fabricated by varying the citric acid concentration. The fabricated ethylcellulose and activated carbon acted as electropositive triboelectric materials and carbon-based electrodes, respectively. Teflon was employed as a reference negative triboelectric layer that was interfaced with an aluminium electrode to realise the TENG properties. The TENGs fabricated with different additives, namely, ethyl cellulose with citric acid, myristic acid, and oil, exhibited unique output of (6.8, 6.6, and 6.4 $\mu W/cm^2$), as compared to other edible devices. In addition to energy harvesting, they fabricated an energy storage device (supercapacitor). Similarly, Chen *et al.* [68] fabricated a microstructured cellulose film (MCF) using hot pressing coupled with screen mesh templating (Figure 3). The electrochemical performance of the MCF pressure sensors was analysed using a universal testing machine for pressure loading, and the output was recorded using an electrochemical workstation. Because the MCF consisted of different mesh numbers, the output varied depending on the mesh number. The MCF paper with a 50–300 mesh exhibited a maximum current under the same pressure, as shown in Figure 3 (a, b). Additionally, the MCF exhibited excellent properties such as flexibility, durability, sensitivity, and wide detection range. Hence, MCFs can be applied to real-time pressure sensors and human motion applications.

Figure 3 (c, d) shows the pressure sensor using a finger to touch the MCF paper. A clear and accurate output signal was generated between the force and interval between the finger pressures. They also investigated the detection of a human wrist pulse using an MCF pressure sensor. As depicted in Figure 3e and f, which show the conditions of before and after exercise, stable sensing signals were observed with the motion of humans. These results indicate that MCFs can be employed in real-time applications, such as wearable devices, healthcare, and motion detection. Chen *et al.* [69] innovatively adopted creep cellulose paper (CCP) and nitrocellulose membranes as friction layers for paper-based TENGs (Figure 4 (a-h). Different microstructures have been employed to improve the efficiency of devices for real-time applications, such as computer keyboards and pianos. The schematic representation of TENG and chemical structure of the cellulose and nitrocellulose depicted in the figure 4 (a-c). The TENG was fabricated with CCP and nitrocellulose material as the positive and tribonegative friction materials, respectively. Field emission scanning electron microscopy (FESEM) indicated that the wave like microstructure as shown in the figure 4c. The output of the device varied according to the thickness and internal structure of the CCP layer as shown in figure 4d. Figure 4 (a-h) shows the output voltage of a paper TENG with different CCP and NCM layers. The output voltage increased from 144.0 to 196.8 V as the number of CCP layers increased from one to three. However, further increasing the number of layers decreased the output voltage (136 V). Additionally, good durability and stability were observed with obvious differences in the output voltage.

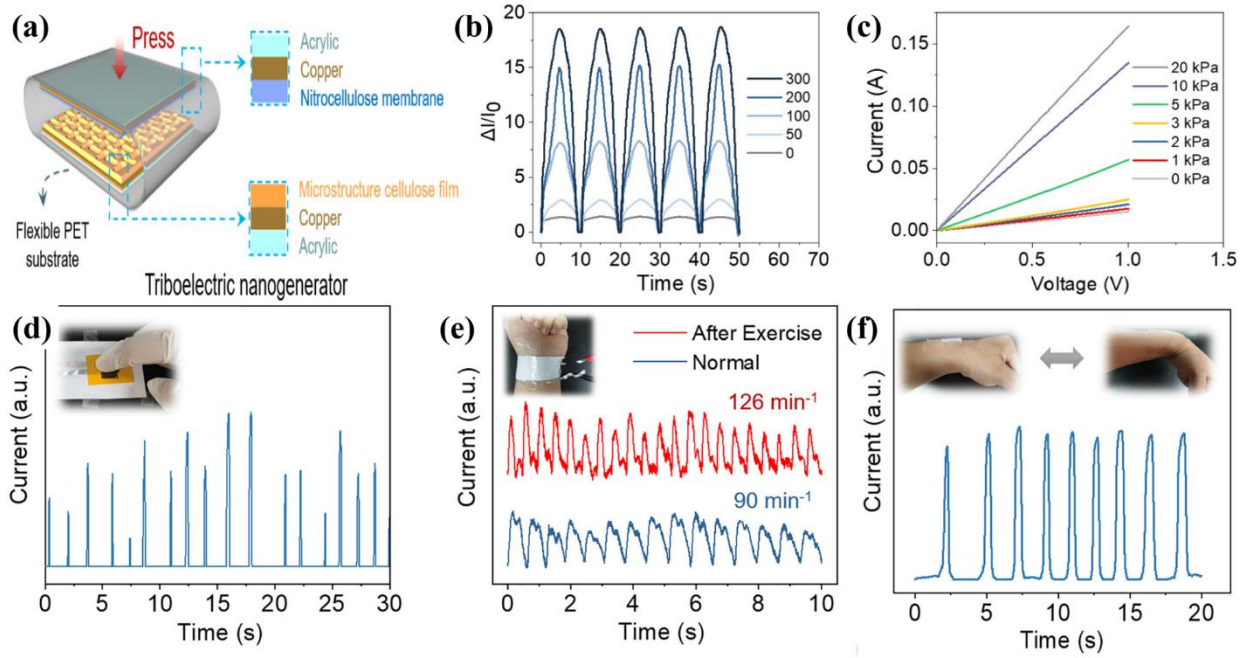

Figure.3 (a) Schematic representation of surface microstructured TENG, (b, c). Electrochemical performance of microstructured carbonized cellulose films with different pressure, (d, e, & f). Current output generated by finger pressure, after exercise and wrist movement. Reproduced with permission. Copyright 2019, Elsevier

Similarly, Kim *et al.* used bacterial nanocellulose to fabricate biocompatible TENGs as shown in the optical image figure 5a. The transparent bacterial cellulose film was extracted by solubilisation. The bacterial nanocellulose film exhibited a higher contact angle than copper foil. The TENG was fabricated with bacterial nanocellulose using various input conditions and structural aspects. When force was applied to the fabricated TENG, the electrons flowed from the copper foil to the bacterial nanocellulose film, which acted as a negatively charged material. A positive output signal was generated under the pressed state because of electron flow in the opposite direction from the bacterial cellulose film to the copper foil. Figure 5 b & c indicated that the bacterial nanocellulose film generated a maximum output of 13 V when in contact with the copper foil, as compared to the PI electrode (7 V). Additionally, different loads were applied to the device without any changes in the device parameters. Furthermore, the device was analysed using different structural modifications of the film (Figure 5 d & e). The curvature and friction area played vital roles in the deformation and fast recovery of the device to its initial state. The 60 mm radius curvature film showed a higher output voltage than the other curvatures.

The results indicate that the performance of the device also depended on the surface curvature or roughness of the film [70].

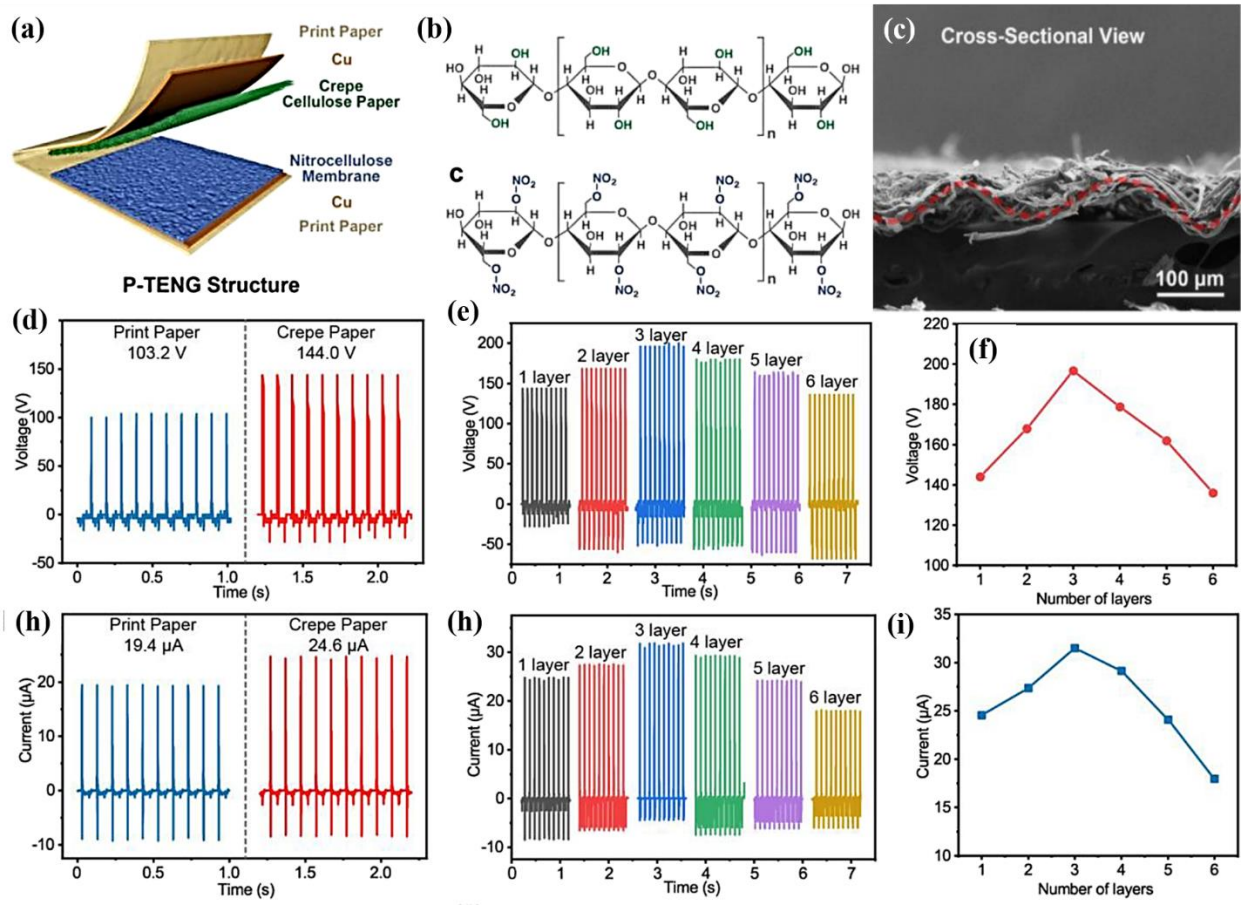

Figure.4 (a) Schematic representation of paper-TENG, (b). Chemical structure of cellulose and nitrocellulose, respectively. (c). FESEM-Cross section of fabricated device, (d-h). Load voltage and short-circuit current of Triboelectric performance of paper-TENG under 10 Hz frequency stress with different layers of cellulose paper. Reproduced with permission. Copyright 2019, Elsevier.

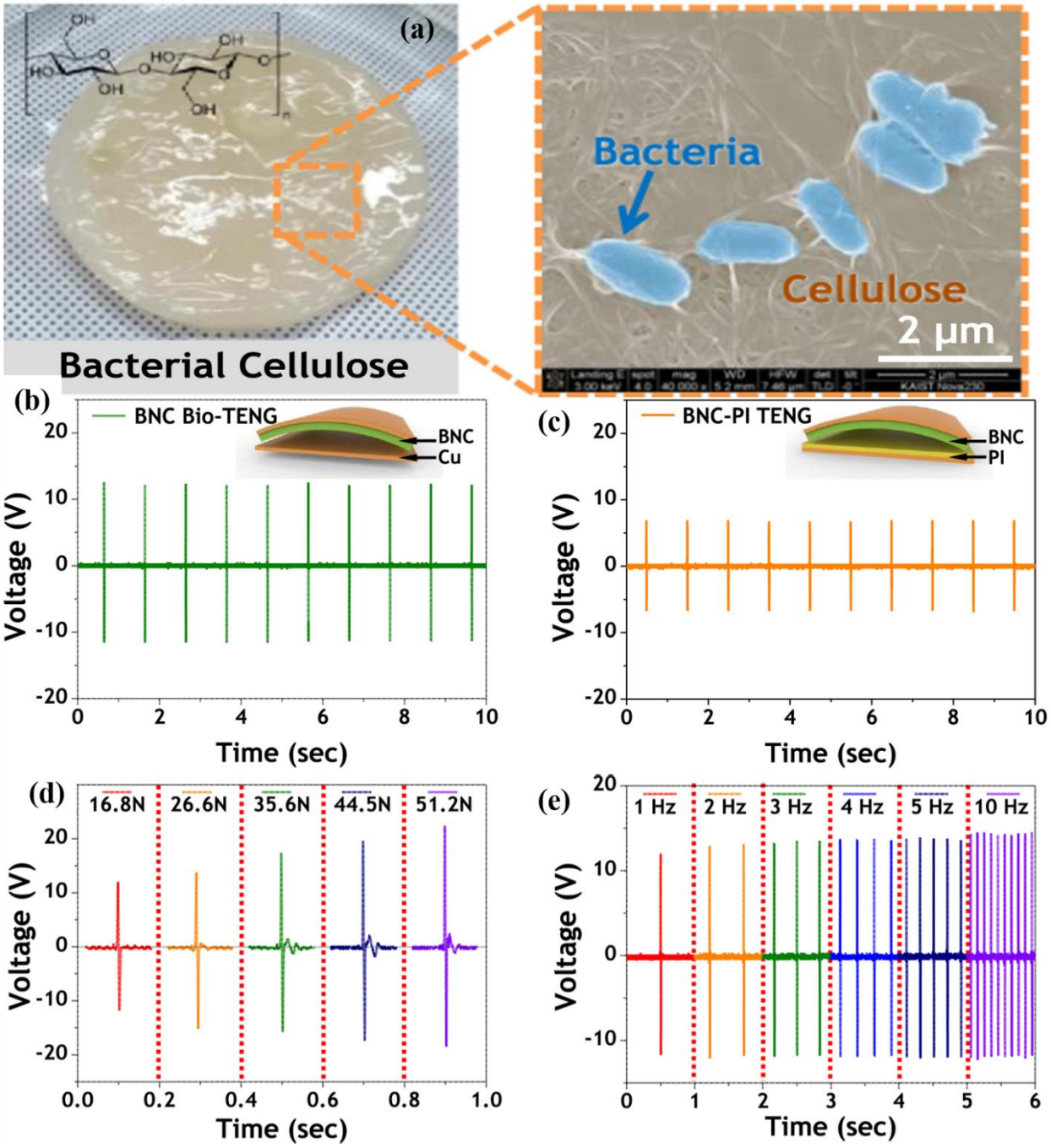

Figure.5 (a). Optical images of bacterial nanocellulose thin film, (b) Performance of Triboelectric nanogenerator under various conditions (b). The output voltage of bacterial nanomaterials contacted with Cu foil, (c). Contact with PI electrode film, (d). Different input pulse conditions with magnitude, (e). Frequency. Reproduced with permission. Copyright 2017, Elsevier.

3.2 Gelatine-based TENGs

Gelatine is a complex peptide molecule composed of 18 different amino acid species that are nontoxic, biocompatible, biodegradable, and inexpensive, and can be derived from a wide variety of sources [71-73]. Moreover, gelatine consists of large amino, carbonyl, and hydroxyl groups, which facilitates good ion transport and acts as a triboelectric material. Hong *et al*. [74] explored the similarities between the skin and switchable ionic polarisation of ion-doped gelatine towards dynamic mechanical stimuli. The fabricated ion-doped gelatine exhibited both triboelectric and piezoelectric effects as shown in figure 6 (a-f). A negative voltage output was obtained when human skin came into contact with the ion-doped gelatine owing to the triboelectric effect, inducing ionic polarity in the ion-doped gelatine to compensate for its surface charge. In contrast, the piezoionic effect induced ion redistribution, which led to switched polarity and generated a positive electrical output (Figure 6b). Furthermore, they performed density functional theory calculations to show the attraction of the ion towards ion-doped gelatine. Figure 6 (c, d) shows the effects of different ion doping concentrations. The results indicated that the piezoionic voltage increased by approximately 44.6%, from 0.522 V (0.2 m LiCl) to 0.755 V (0.4 m KCl). Additionally, they touched an object with perfluoroalkoxy alkane (PFA) and a nylon film. PFA films are well-known tribo negative materials, with an output of approximately 4.72 V. However, the output voltage was slightly reduced to 2.86 V when the PFA film was rubbed with sandpaper. The nylon-based films exhibited a very low output voltage of -10.52 mV, which was further reduced using nontextured nylon films (Figure 6 (e, f)). This effect was observed because of the reduced surface area which prevented electron transfer between the materials. The ion-doped gelatine exhibited excellent properties for dynamic tactile sensing with rapid changes in force, skin compliance, and structural flexibility. Hence, they developed a wearable dynamic sensing-based communicator (WDC) that was used to control the movement of a miniature car as a prototype. The WDC was fabricated using a 0.2 m KCl-doped gelation film with an integrated circuit board and Bluetooth module. The movements of the vehicle were controlled using the fabricated device, which showed that increased movements could be effortlessly controlled [74]. Similarly, Min *et al*. [75] demonstrated a stretchable TENG with freezing tolerance and a strain sensor with a stable and highly conductive gelatine/NaCl organohydrogel. The gelation/NaCl-based hydrogel was fabricated using a simple, facile immersion strategy in glycerol/water.

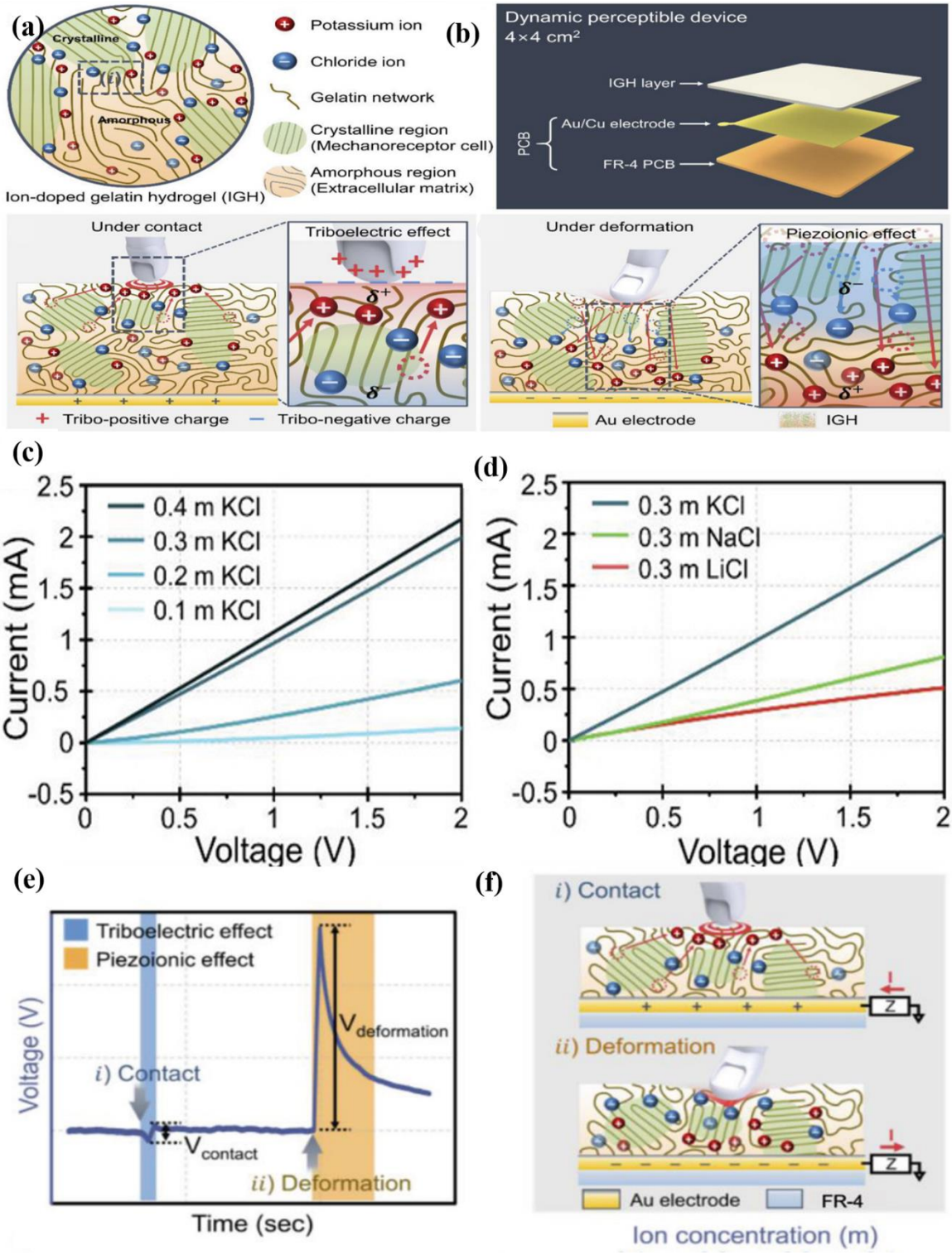

Figure. 6 Schematic representation of (a) KCl ion distribution, (b). the fabricated gelatin-based device under triboelectric and piezoionic effect, (c). I-V analysis of gelatin with

different KCl concentrations, (d). with different metal ions, (e). Output characteristic peaks. $V_{contact}$ and $V_{deformation}$ denote voltage output under contact and deformation, respectively, (f). Schematic representation of operation mechanism. Reproduced with permission. Copyright 2021, Advanced Functional Materials, John Wiley and sons.

The transparency and self-healing properties of the gelatine/NaCl were comprehensively studied. The gelatine/NaCl organogel exhibited an excellent 91% transmittance value at 600 nm owing to the inhibition of the phase separation of the gelatine network. The organogel also exhibited superior flexibility and mechanical strength owing to its multiple cross-linking effects, such as ionic and hydrophobic interactions induced by the salting out effect. The self-healing capability of the gelation/NaCl organogel was impressive and extraordinary. Self-healing was confirmed by using a light-emitting diode (LED) closed circuit with two pieces of gelatine. After the gelatine completely self-healed, LED was lit up. The gelation/NaCl self-healed because of the formation of new hydrogen bonds, ionic interactions, and hydrophobic aggregation between the gelation/NaCl cut materials. They also demonstrated a wearable sensor to monitor human motion in healthcare applications as a real-life application demonstration. The hydrogel was installed on the human hand to study human hand movements, such as hand, wrist, and elbow bending. The results showed that gelatin/NaCl is an excellent candidate in the field of wearable electronics. The anti-freezing TENG showed an excellent open-circuit voltage (V_{oc}) of 420 V with a short-circuit current of 12 A and charge transfer of 180 nC. They also investigated the ability of the TENG to harvest energy with different external voltage loads, and a maximum output voltage of 0.8 W/m^{-2} was observed for the applied load. Moreover, a self-power-based anti-freezing gelatin/NaCl organogel was demonstrated for human-machine interactions.

Min Wu *et al*. [75] fabricated a flexible and multifunctional fish gelatine TENG composed of PTFE/PDMS and fish gelatine. Fish gelatine was extracted from fish scales, which was cleaned and treated with diluted hydrochloric acid to remove minerals from the gelatine. The fabricated fish gelatine TENG consisted of two parts, namely, a PTFE/PDMS composite with copper foil and a piece of print paper and a fish gelatine film with a rough surface. The fish gelatine thin film was chosen to study the triboelectric effect because of its strong ability to lose electrons during triboelectrification. They investigated the effect of the surface area by varying the surface of the fish gelatine film. Figure 7 shows that the rough film exhibited an enhanced output voltage (125 V), as compared to a smooth film (20 V), which indicates that the roughness

of the film drastically increased the friction between the materials and led to an enhanced electric charge output. Additionally, they employed the fish-gelatine TENG to perform self-powered sensing. The fish gelatine TENG was used to monitor human motions, such as finger bending and wrist movements (Figure 7 (a-c)). Moreover, the monitoring of shallow or deep breathing indicated that the fish gelatine TENG could distinguish between each action. A 5 × 5 fish-gelatine TENG could directly light up 50 LEDs with an output voltage of 130 V (Figure 7 (d-f)). Additionally, the fish-gelatine TENG exhibited enhanced performance, low cost, and superior flexibility in the field of portable, wearable, and biodegradable electronics [76] .

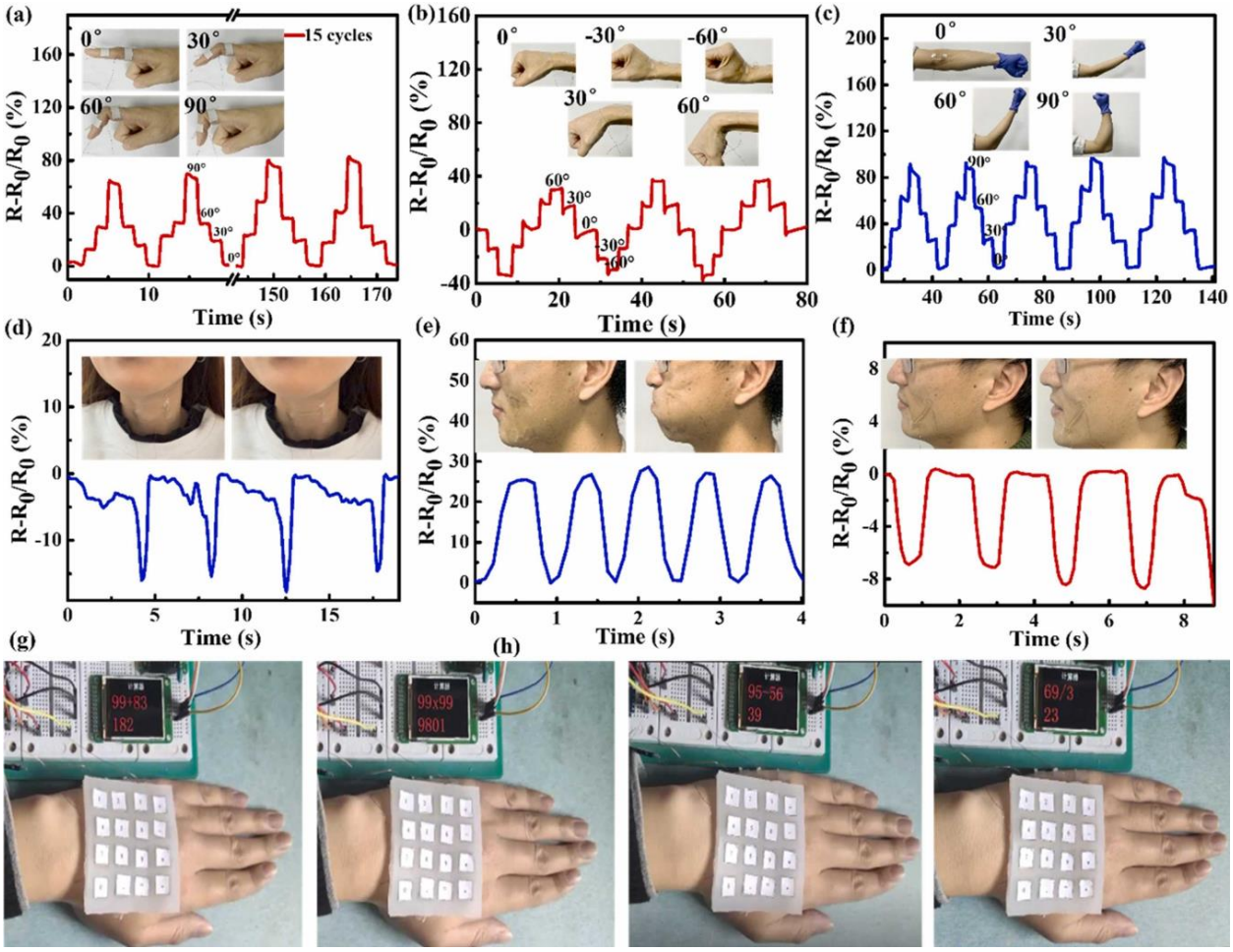

Figure 7 (a-f). Real-time application of fabricated devices under various human motions like finger bending, wrist bending, elbow bending, swallowing, pouting and smiling, (g, h). Calculation demonstration with the fabricated device. Reproduced with permission. Copyright 2022, Nano Energy, Elsevier.

3.3 Chitosan-based TENGs

Chitosan is a flexible and biocompatible cationic biopolymer that exhibits electrostatic interactions with oppositely charged ions and molecules. Additionally, the chitosan structure is identical to the cellulose structure and can donate an electron from its large number of OH and NH_2 groups; it can be utilised as a positive TENG [77-79]. Charoonsuk *et al.* demonstrated a chitosan-incorporated protein-based TENG as shown figure 8 [80].

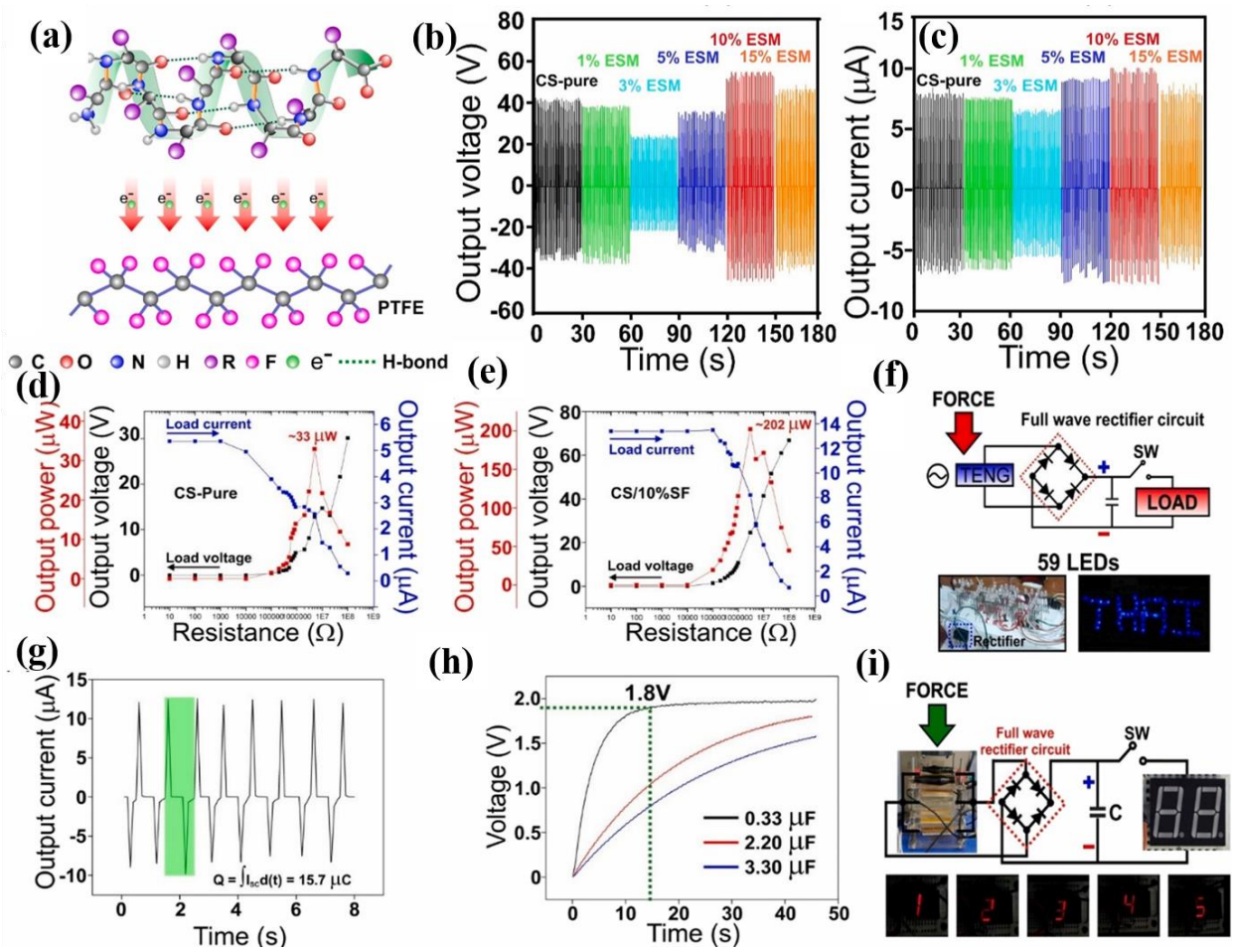

Figure 8 Schematic representation of electron transportation between the protein molecular structure and PTFE, (b, c). Output voltage and current of Chitosan/ESM device, (d). Pristine chitosan output voltage, (e). Chitosan/SF composite @ different load resistance, (f). Practical application using full wave rectifier, (g, h). Transferred and chargeability of chitosan/SF film (10%), (i). Practical application with 7 segment LED. Reproduced with permission. Copyright 2021, Nanoenergy, Elsevier.

A composite of chitosan/protein films was fabricated using a simple casting method. The FTIR spectra of the composite showed the presence of CH-OH, CH_3, C-O, C-O-C, COO^-, and OH bending. The V_{OC} and ISC with varying protein fillers were analysed using a vertical C-S TENG. Figure 8 (b-f) shows that the TENG exhibited an enhanced maximum output of approximately 55 V and 10 μA at 10% loading of an eggshell membrane. However, an increasing concentration of silk fibroin exhibited a decreased output voltage, which may be due to the agglomeration and non-uniform distribution of the filler into the chitosan matrix. The mechanism can be explained by two major phenomena, namely, triboelectrification and electrostatic induction. Initially, an external force was applied to the TENG, and charge transfer was induced between the triboelectric materials owing to the different electron affinities. Chitosan/proteins donate electrons to the strong electron capture ability of PTFE. When the force is released, the induced charges flow back in the opposite direction when an external load is applied (Figure 8i). Additionally, the biodegradation was extensively studied, and the results indicated that the chitosan can be completely degraded. The chitosan composite with silk fibroin exhibited excellent output even after 70% degradation of the weight film, demonstrating the stability and biocompatibility of the chitosan composites in the environment.

Similarly, Kim *et al*. [81,82] fabricated a wearable and eco-friendly chitosan-diatom TENG. Diatoms are aquatic, unicellular algae that reproduce through photosynthesis. Owing to their abundance and low cost, diatoms offer almost endless potential for use as multifunctional biomaterials. Additionally, diatoms can absorb carbon dioxide molecules and release oxygen through photosynthesis. A vertical contact separation technique was used to realise the triboelectric effect in a chitosan–diatom composite film (positively charged) with an FEP film (negatively charged) (Figure 9). When both the films came into contact, a charge difference was created between them to balance the Fermi level. The potential difference increased when the force was released from the counter electrode, leading to the flow of electrons from the FEP film to the chitosan diatoms. In contrast, electrons flowed from the chitosan diatom to the FEP film. Figure 9b shows the maximum output generated by the chitosan-diatom (0.1 %) composite, as compared to that of other compositions. An output of approximately 150 V was observed for a 0.1% diatom composition, and the output voltage decreased as the diatom composition increased.

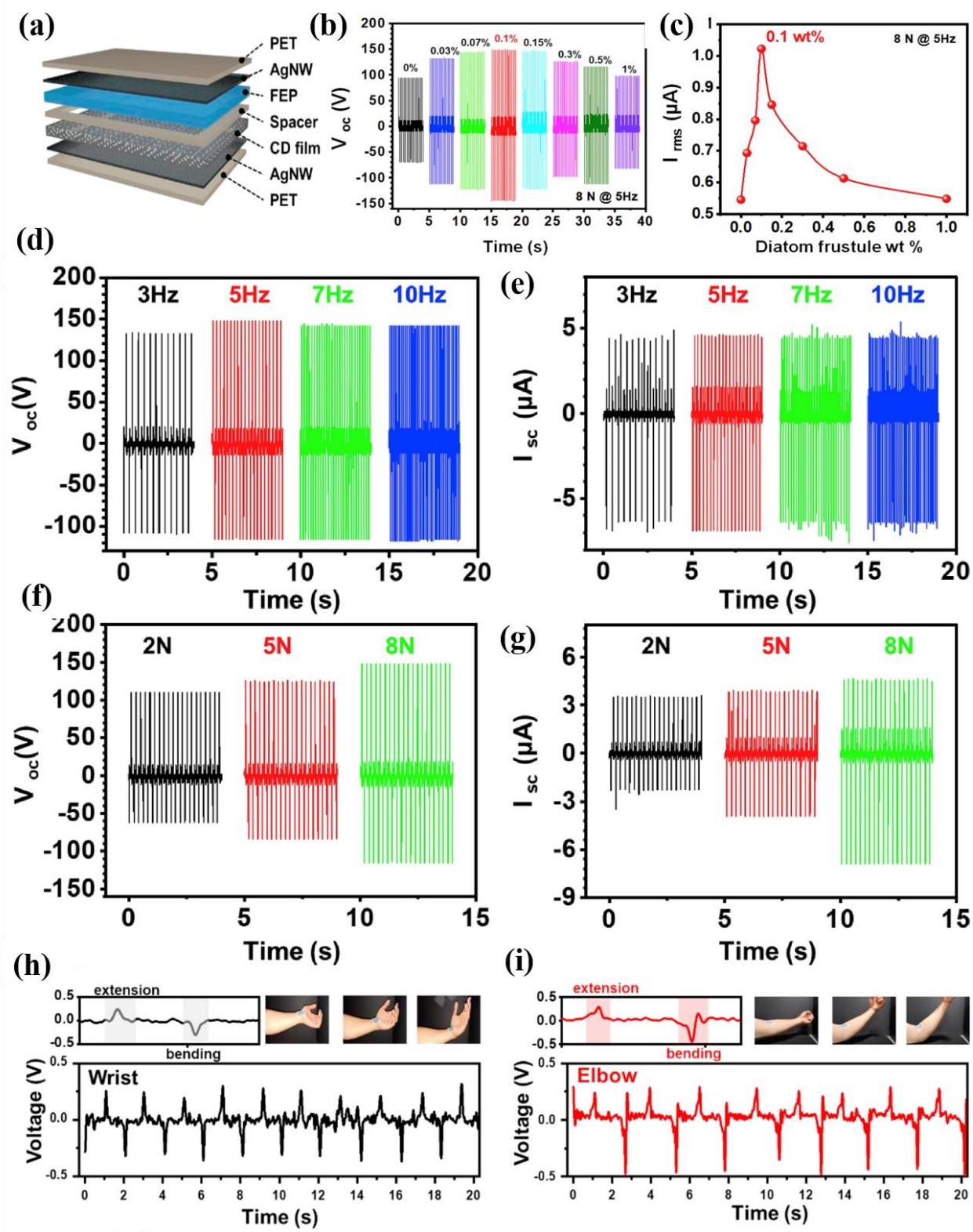

Figure 9 (a). Schematic configuration of fabricated chitosan-diatom TENG, (b). The output of open circuit voltage of the device, (c). Short circuit current depending on the diatom

weight percentage, (d-g). Power generation of the fabricated device with different frequencies, (h, i). The output response of the device operated from human motions. Reproduced with permission. Copyright 2020, Nanoenergy, Elsevier.

The work function of the device changed depending on the diatom concentration, as shown in the Figure 9 (c-e). Figure 9 f &g shows the voltage and current output based on different pressure. Additionally, they analysed the intracutaneous reactivity of chitosan-diatom mixtures. The results indicated that the chitosan-diatom composites fulfilled the global biosafety standards. Further, the fabricated TENG was attached to the human body (wrist, elbow, knee, and ankle) to study the motion of these body parts (Figure 9h and i). The results indicated that each motion could be distinguished and was reproducible. To improve the performance of TENGs and monitor Parkinson's disease, Kim *et al.* fabricated a self-healable catechol-chitosan-diatom TENG (Kim et al., 2021). The TENG could detect low-frequency vibrational motions in Parkinson's patients without any batteries. Furthermore, this film exhibited both hydrophilic and hydrophobic properties. The TENGs for diagnosing Parkinson's disease were fabricated using catechol-chitosan-diatom and M-shaped films. An M-shaped Kapton film was introduced to enhance the sensitivity for detecting Parkinson's disease. Figure 10 (a-d) shows the electrical output of the fabricated catechol-chitosan-diatom and M-shaped films. A force of 8 N with a movement frequency of 3 Hz was applied to the fabricated device using a mechanical shaker. The device exhibited a maximum output of 110 V and a short circuit of 3.8 μA. The fabricated device was used to examine patients with Parkinson's disease and was operated in the C-S mode. The tremor sensor attached to the wrist of Parkinson's disease patients produced a sufficient output voltage signal, as depicted in Figure 10. Furthermore, COMSOL Multiphysics was used to investigate the working mechanism of the TENG. The device showed a maximum output when the electrode materials were separated from each other. The tremor sensor showed a maximum output of 4 and 1.7 V for minor tremor analysis (Figure 10e). Additionally, high-frequency components revealed that 4.2, 5.7, 7.3, 9.2, and 10.3 Hz were found in severe tremors and the signal power increased as the tremor motion increased. The above results indicate that Parkinson's disease could be detected using the fabricated tremor sensor.

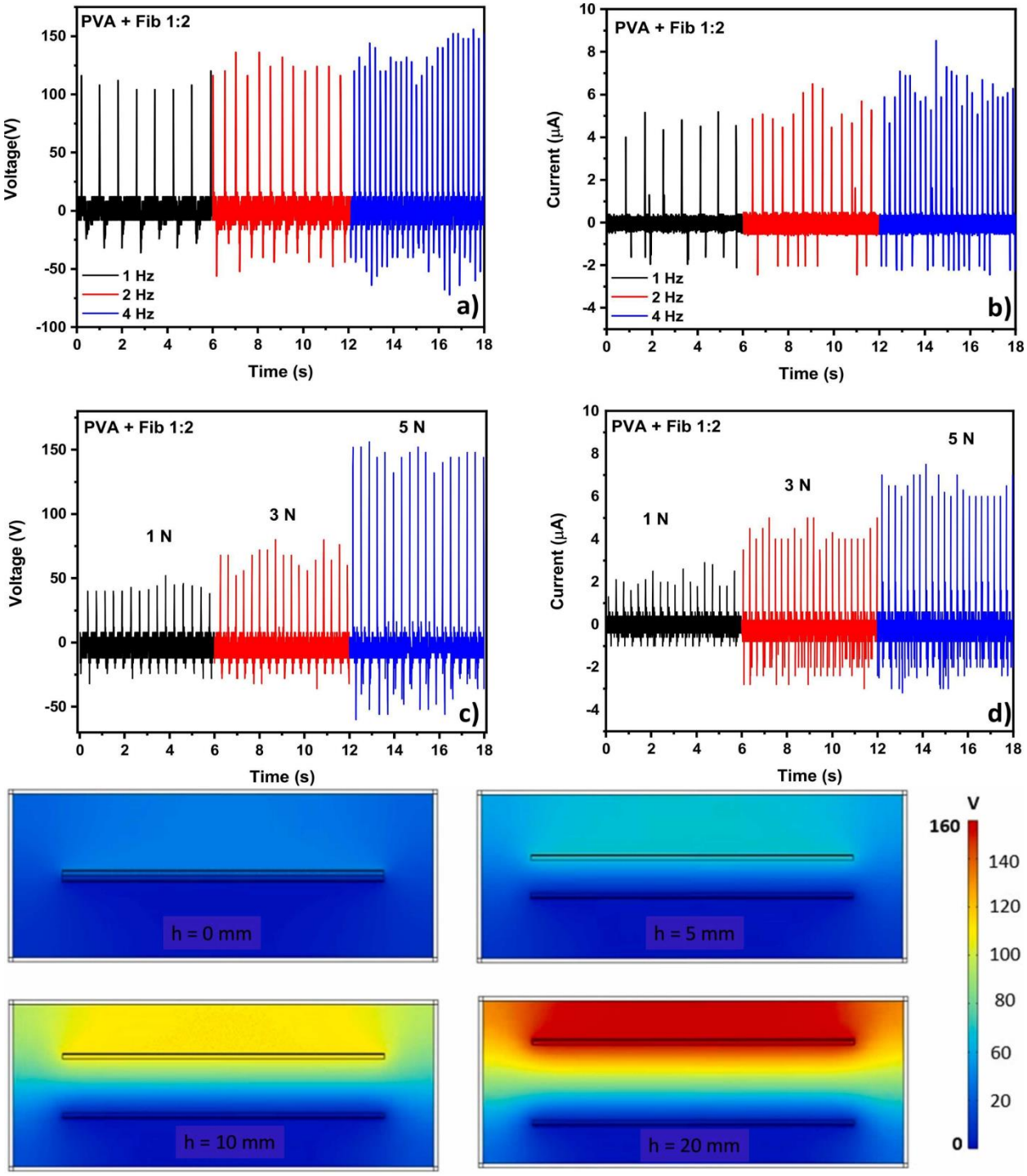

Figure 10. (a, b). The output of the device under various frequencies, (a, d) Open and short circuit current under influence of force, (e). Comsol simulation of PVA+Fibroin with different distances between the triboelectric materials. Reproduced with permission. Copyright 2023, Nanoenergy, Elsevier.

3.4 Silk-based TENGs

Silk is a well-known and abundant animal fibre used by humans. Silk can be extracted from arthropods, such as scorpions, spiders, and chrysalises, using a solidification process. Silk is composed of proteins, sericin, and Silk fibroin (SF), and has an extraordinary tensile strength and toughness [83,84]. The excellent properties of silk are attributed to the proteins linked to the peptide block by hydrogen bonding. Silk is widely used in the textiles industry. Early reports indicated that modified silk could be used in energy storage, energy generation, and wearable electronics owing to its good conductivity and biocompatibility.

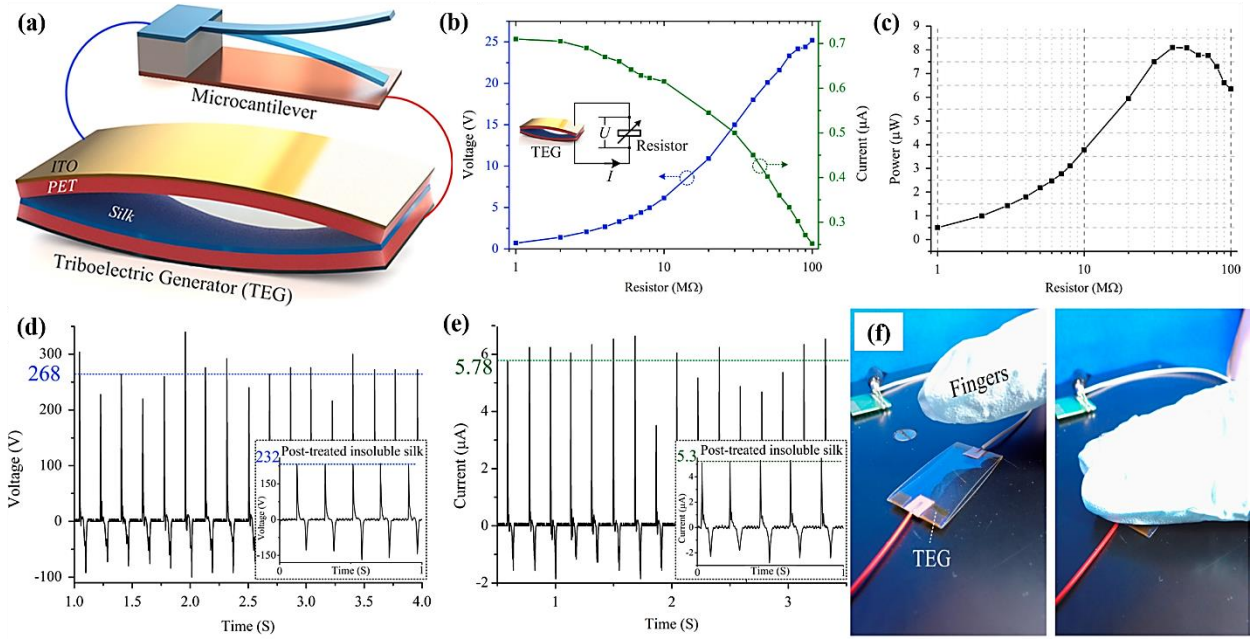

Figure 11 (a). Schematic representation of the fabricated device, (b). Output and current performance of the device under 5 Hz stable vibration, (c). The maximum output is obtained when the load resistance equals the internal resistance, (d, e). Output voltage and current obtained while pressing the device with the human finger, (f). Optical image of the driving the TENG by finger. Reproduced with permission. Copyright 2016, Nanoenergy, Elsevier.

For example, Candido *et al*. developed a novel and simple TENG fabricated using a poly(vinyl alcohol) (PVA) and silk fibroin composite as a positive triboelectric layer [85]. The thermal stability of silk fibroin was analysed using thermogravimetric analyses, as shown in Figure 11a. The strength and strain of the PVA increased with increasing concentrations of silk fibroin. The fabricated TENG was tested at different frequencies (1, 2, and 4 Hz) and forces (1, 3, and 5 N). The PVA/silk fibroin exhibited a high voltage (161 V) and current (6.8 μA), as

compared to other composite materials. To understand the mechanism responsible for this, COSMOL software was used to systematically study the distribution of the potential on the surface of the electrodes. The maximum output was 157 V at a distance of 20 mm between the electrodes, which shows that more electrons accumulated on the more negative electrode materials. Additionally, the obtained AC output was converted into a direct current (DC)-pulsed output signal. The device showed excellent durability and cyclability of 40,000 cycles at 4 Hz (Figure 11 b-c). Similarly, Zhang *et al.* fabricated a silk fibroin-based TENG to simulate an autonomous sensor network (Zhang et al., 2016). The roughness and chemical composition were improved by using oxygen plasma etching. The silk fibroin device exhibited an enhanced transmittance of 90% and also showed a good contact angle, as depicted in the figure11. The fabricated silk fibroin TENG exhibited a high output voltage (268 V), power density (193.6 $\mu W/cm^2$), and current (5.78 μA) at an applied load of 40 MΩ. Additionally, it exhibited extraordinary durability and a stable output for over 18000 cycles (Figure 11 d-e). The optical image of pressure applied by human finger was shown in figure 11f.

Furthermore, silk fibroin TENGs to drive micromechanical devices and optical displays were investigated. The device was operated by a human finger and generated electric power to light two 4-bit liquid-crystal and LED displays. The device exhibited a decreased output voltage as the humidity increased. Moreover, the output saturated at a 60% humidity level, and became unstable at humidities exceeding this. Niu *et al.* [86] demonstrated a pulse-driven silk-nanoribbon bio-TENG fabricated using nascent silk nanoribbons and regenerative silk fibroin films. The 0.38 mm-thick silk nanowires were exfoliated from natural silk. Transmittance analyses showed that the transmittance increased with an increasing nanowire thickness. However, the silk nanoribbon became brittle when the nanowire thickness increased. The synthesised silk nanoribbons could be easily degraded using an ethanol and methanol treatment, but the duration of degradation depended on the post-treatment or addition of enzymes to the film. Moreover, the major component of silk fibroin is composed of peptides and amino acids, which do not affect the human body. The fabricated silk nanoribbon bio-TENG exhibited a maximum output voltage and an approximate current density of 41 V 0.5 μA, respectively. The silk fibroin exhibited excellent output even with light forces owing to the nanoribbons. Hence, silk nanoribbons were used for the real-time monitoring of different movements of the human body. The TENG showed an impressive response to finger, footstep, and elbow movements.

Additionally, the signals could be easily distinguished. The above results indicate that silk fibroin nanoribbons can be an attractive energy source that can be used in implantable self-powered sensors such as pacemakers and detectors.

4. Implantable biocompatible and biodegradable nanogenerators

Implantable medical devices require certain properties, such as biocompatibility, biodegradability, long life, durability, and excellent dependability. Implantable devices can be implemented to improve next-generation healthcare devices [87-88]. Most devices monitor physiological signals and electrical stimuli. However, implanting and removing a self-generating triboelectric from the human body requires surgery. To avoid surgery and the cost of the operation to remove the device, a new type of implantable biodegradable electronic devices that can be absorbed or degraded *in vivo* is required to avoid invasive secondary surgeries. Li *et al*. fabricated an implantable and ultraflexible nanogenerator, which converted muscle movement into an output signal *in vivo* during breathing. A sliding mechanism-based nanogenerator was used with a soft silicone elastomer as the packing layer. The biocompatibility of the fabricated device was tested using a 3T3 fibroblast cell viability test on the surface of the packaging materials. The device was implanted inside the diaphragms of rats, which exhibited an excellent *in vivo* biomechanical energy harvesting ability, producing a steady DC output with a voltage up to 2.2 V. The device continuously powered an LED without any delay or decay in power as a battery-free device [89].

4.1 Ultrasound-based implantable and biodegradable TENGs

Ultrasound is one of the most widely used techniques in industry, military, medical imaging, and photocatalysis. Ultrasound-based devices are widely used because of their major advantages, namely (i) smaller attenuation than electromagnetic radiation, (ii) shorter wavelength, allowing it to be focused on a millimetre scale with excellent spatial resolution, and (iii) safety to the human body during medical diagnostic applications according to the Food and Drug Administration. However, the intensity of the ultrasound should not exceed 720 mW cm^{-2} [90-92] Therefore, researchers have focused on ultrasound-based implantable TENGs.

Imani *et al.* demonstrated an ultrasound-based implantable and biodegradable TENG. Additionally, they studied the elimination of microorganisms using electrical stimulation. Figure 12 (a-h) shows a schematic representation of the design and output performance driven by ultrasound under the skin of the fabricated TENG. Moreover, the TENG was fabricated with

biocompatible and biodegradable poly (3-hydroxybutyric acid-co-3-hydroxyvaleric acid) to act as an encapsulation and vibration layer. Figure 12c indicated that the voltage increase with increase in the probe power. Initially, the TENG was kept in water with different distances between the TENG and the ultrasound probe as shown in figure 12 d-f. A voltage of approximately 4 V at 40 MΩ and a current of approximately 22 μA at 1 Ω were observed under these conditions. The antibacterial effect of the fabricated TENG was investigated using an *ex vivo* experiment. The TENG exhibited a voltage of 2.2 V at an impedance of 40 MΩ and a current of 11.7 μA Figure 12 g-h. Bacterial survival was studied using porcine tissue with fat and muscle layers. The TENG was placed under the contaminated skin and was covered with the porcine skin, as shown in Figure 12d. The results indicated that 92 and 86% of *S. aureus* and *E. coli* were inactivated. Additionally, the TENG was completely biodegradable within the body itself, and there was no need for surgery to remove the device [93].

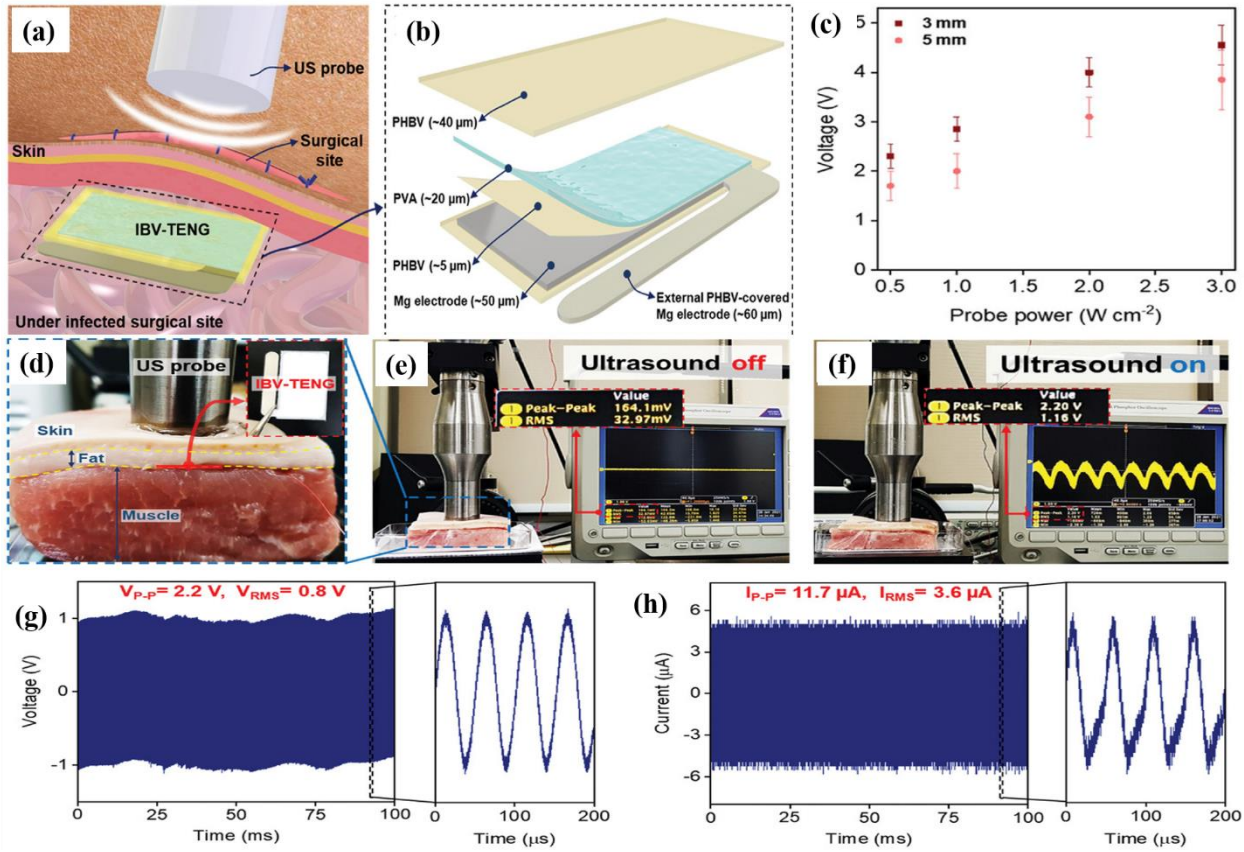

Figure 12 Schematic representation of IBV-TENG operated by ultrasound under the skin, (b) Schematic illustration of fabricated device, (b). The output of the device was obtained with different distances of the ultrasound probe (3 and 5 mm), (d-f). Optical image of IBV-

TENG inside porcine operated with ultrasound, (g & h). Output voltage and current obtained with 5 mm distance ultrasound probe. Reproduced with permission. Copyright 2022, Advanced Science, John Wiley and Sons.

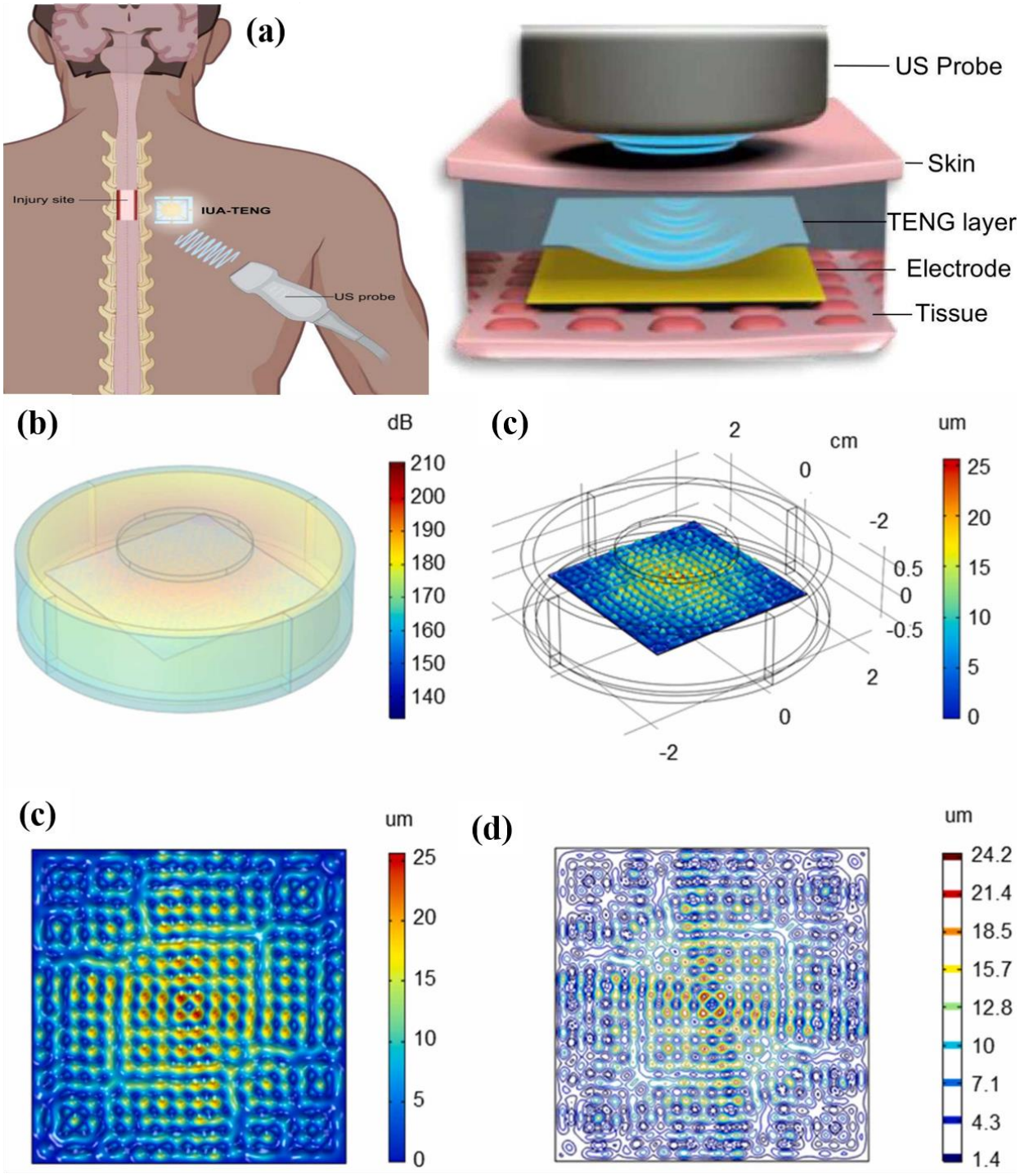

Figure 13 (a). Schematic illustration of ultrasound probe irradiating the implanted device, (b). 3D simulation results of acoustic pressure distribution under ultrasound irradiation,

(c). Resultant node and antinodes on the triboelectric layer, and (d). Displacement of triboelectric layer. Reproduced with permission. Copyright 2022, Nano Energy, Elsevier.

Another group fabricated a bio-adhesive TENG to heal wounds using ultrasound. The TENG was fabricated with a biocompatible material and a bioadhesive layer to realise the ultrasound effect inside the wet tissue. When ultrasound was applied to the fabricated TENG placed in water, the TENG exhibited an excellent and stable output of 1.50 V and a current of 24.20 μA under 20 Hz ultrasound. Blood loss was reduced by approximately 82%, and the skin was sealed using a strong ultrasonically simulated applied field. Additionally, *in vitro* experiments were performed to demonstrate the migration and regeneration of tissues by the electric field. In real-time applications, the device was utilised to heal rat skin wounds with an ultrasonically produced electric field [94]. These reports indicate that TENGs can be used in various biomedical applications.

Similarly, Deng *et al*. [95] conducted a computational investigation on ultrasound TENGs as depicted in figure 13a. Using COMSOL, different nylon layer thicknesses were modelled to study the absorption of the ultrasound layer. Figure 13 b-c shows the simulation results of the acoustic field distribution with and without a triboelectric layer. The results were quantified for different thicknesses of the ultrasound probe and triboelectric materials. Ultrasound exhibited a square triboelectric layer that was positively correlated with size, and the physical parameters were simulated and calculated. Figure 13 c-d shows the distance-dependent effect based on the sound field propagation. The results indicated that wireless powering techniques can be employed in various fields.

4.2. Implantable TENGs in nerve stimulations

TENGs have been recently utilised in the field of neuromodulation to simulate or activate central nerves such as the brain, spinal cord, muscles, and peripheral nerves. Moreover, a significant breakthrough in body weight control using neuromodulation has been achieved, leading to the development of novel anti-obesity strategies [96,97]. Implantable neuromodulation has become an important method for leg simulation, weight control (vagus nerve), and other therapies [98]. The major issues of neuromodulation are tissue damage and the use of biocompatible electrodes.

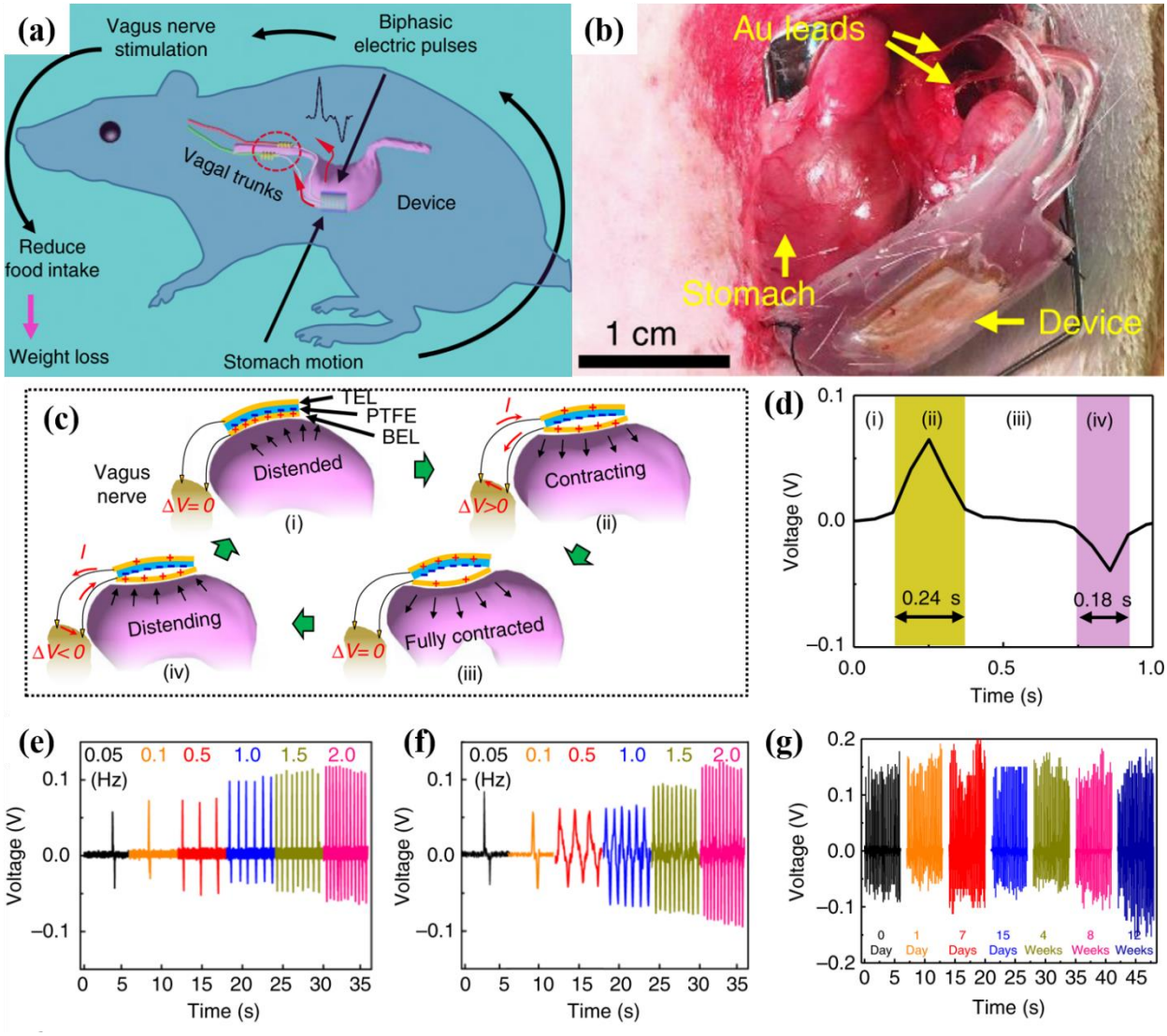

Figure 14 a. Schematic representation of implanted device inside the rat, b. Optical image of the implanted device, c. Schematic illustration of working principle of VNS device under stomach movements, d. The single cycle voltage corresponding to stomach movements, e. The output of the device under different agitation frequencies, f. The output of the device connected to the vagus nerve, g. Stability of VNS device. Reproduced with permission. Copyright 2022, Nature Communication, Springer Nature.

Yao *et al*. [87] demonstrated battery-free implantable nerve stimulation correlating to stomach movement. Figure 14a-c illustrates the implanted vagus nerve system on the surface of the stomach. The pulsed electrical output generated by the movement of the stomach stimulates the vagus nerve. The weight of the rat or human body can be controlled by a pulse generated by the

electrical output to restrict food intake. The implanted vagus nerve simulator exhibited an excellent voltage signal of 0.05–0.12 V with corresponding frequency variations (0.1, 0.5, 1.0, 1.5, and 2.0 Hz) (Figure 14d-f). Additionally, electrophysiological signals were analysed for a period after device implantation. Electrophysiological signals were detected in the vagus nerve without external stimulation. The amplitude increased as the vagus nerve stimulation device activated from approximately 0.8–19 mV. These results indicate that the vagus nerve stimulation device can effectively stimulate the nerve without any delays. Furthermore, the stability of the implanted device was investigated under the normal daily activities of the rats. The results indicated that there was no shift in the movement or biocompatibility of the device. The weight of the rats with the vagus device, as compared to that of the rats without the device, was maintained and slightly reduced. Similarly, Chen *et al*. demonstrated the use of implantable graphene/hydrogel nanogenerators for effective vagus nerve stimulation using ultrasound pulses to generate electrical pulses. The device exhibited a maximum output power of 30 mW/cm^2 and a current of 1.6 mA with an applied 0.3 W/cm^2 ultrasound power density. The output generated was comparable to that of commercial bulky neurostimulators and could stimulate the vagus nerve in the human body [99]. Similarly, Lee et al. [100], fabricated a flexible, stretchable, and implantable triboelectric nanogenerator for the stimulation of static nerve recording and simulation, with the main aim of controlling muscle contraction. The research demonstrates effective control of muscle contraction in rats by stimulating the sciatic and common peroneal nerves, suggesting that this technology could lead to the development of wearable, battery-free neuromodulators. The study emphasizes the potential of TENGs for future implantable and sustainable biomedical applications. Figure 15a illustrates the TENGs connected to a sling electrode for stimulating the sciatic nerve, showing more effective activation of the tibialis anterior (TA) muscle (Figure 15b). Figure 15c depicts the electrode implanted on the common peroneal nerve, with the TENG tapped at different frequencies by hand while nerve stimulation was recorded. The compound muscle action potentials (CMAPs) for the TA muscle increased to 6164 μV at 4 Hz, while the gastrocnemius medialis (GM) muscle reached 1720.3 μV, attributed to the increased impact force from higher tapping frequencies due to natural hand behavior (Figure 15d-g).

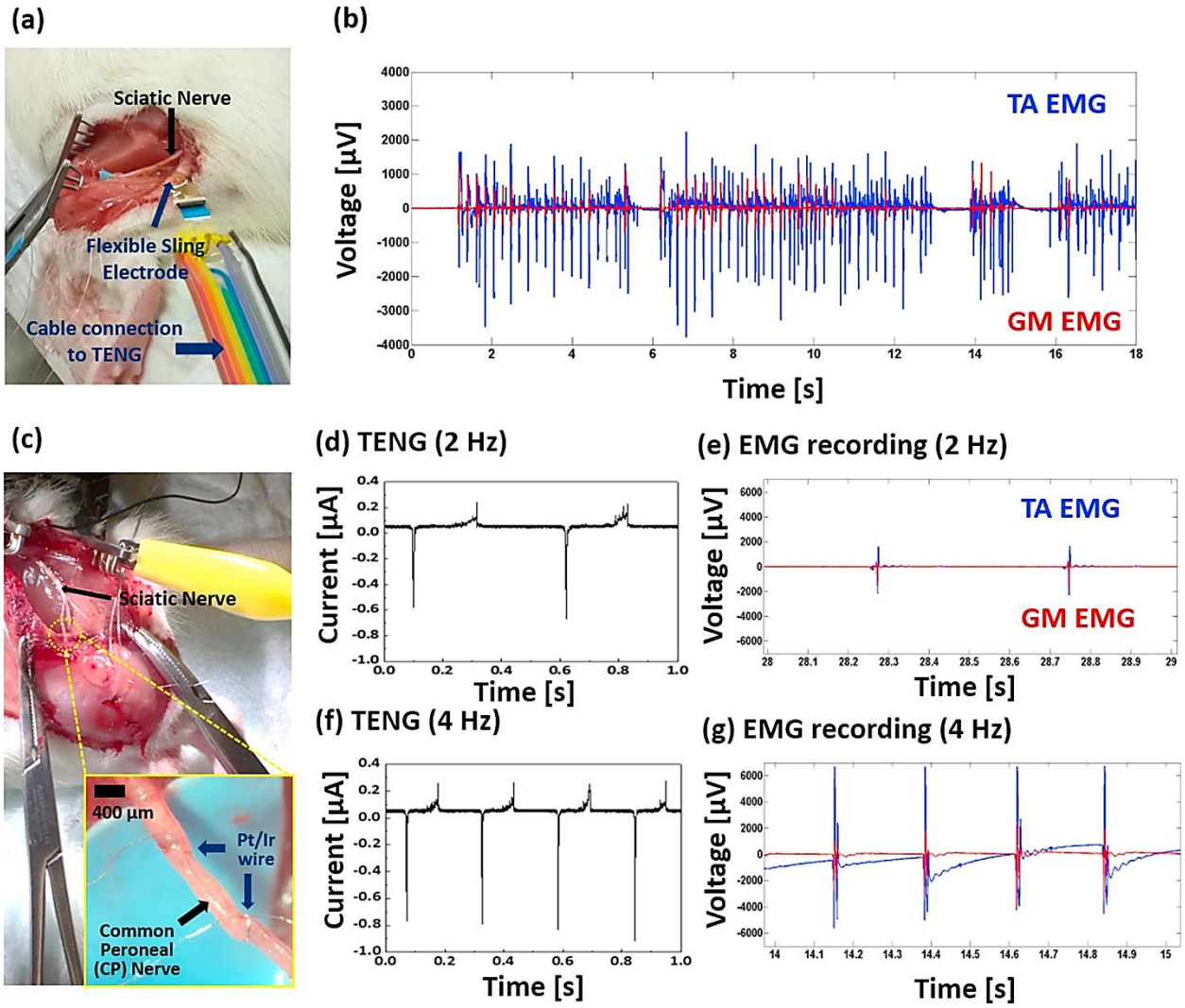

Figure 15a Optical image of in vivo simulation using sling interface and TENG, b. Recorded output of TA muscles by battery-free sling interface, c. optical image of device implanted on common peroneal nerve, d-g. Current peaks generated by TENGS and CMAPs recording at different frequencies. Reproduced with permission. Copyright 2017, Nano Energy, Elsevier.

5. Summary and Outlook

This paper provides a comprehensive review of the current advancements and fabrication techniques concerning biocompatible and biodegradable Triboelectric Nanogenerators (TENGs) utilized in energy harvesting, biomedical, and sensing applications. The heightened focus on

biocompatible and biodegradable materials in the energy and electronics sectors arises from the escalating challenge posed by the accumulation of electronic waste (e-waste). In particular, the significance of biocompatible and biodegradable TENGs is underscored within wearable and implantable medical applications. Nevertheless, further endeavors are warranted to enhance our understanding and identification of bio-derived-material-based implantable TENGs. Moreover, the integration of flexible energy storage technologies with TENGs is anticipated to usher in the next generation of wearable devices for human health monitoring. Ultrasound-based biodegradable TENGs hold promise in mitigating surgical costs and supplanting battery-based implantable sensors. The development of biocompatible and biodegradable wearable and implantable devices becomes imperative when considering their temporary nature. Additionally, there is a need for the advancement of single-electrode-based elastic skin TENGs to cater to feature electronics requirements.

Conflict of Interest

The authors declare that they have no known competing financial interests or personal relationships that could have appeared to influence the work reported in this paper.

Acknowledgement

This research was supported by Institute for AI and Beyond for the University of Tokyo, JST, CREST Grant Number JPMJCR22O2, Japan, AMED under Grant Number JP22zf0127006, JSPS KAKENHI Grant Number JP20H05651, JP22K18804, JP23H04099, 21K14510 and the National Natural Science Foundation of China (No: 62264015).

Reference

1. Shi M, Wu H, Zhang J, Han M, Meng B, Zhang H. Self-powered wireless smart patch for healthcare monitoring. Nano Energy. 2017 Feb 1;32:479–87.

2. Wang X, Liu Z, Zhang T. Flexible Sensing Electronics for Wearable/Attachable Health Monitoring. Small, 2017 Jul 1, 13(25):1602790.: https://onlinelibrary.wiley.com/doi/full/10.1002/smll.201602790

3. Yi F, Ren H, Shan J, Sun X, Wei D, Liu Z. Wearable energy sources based on 2D materials. Chem Soc Rev, 2018 May 8;47(9):3152–88. https://pubs.rsc.org/en/content/articlehtml/2018/cs/c7cs00849j

4. Lou Z, Li L, Wang L, Shen G, Lou Z, Li L, et al. Recent Progress of Self-Powered Sensing Systems for Wearable Electronics. Small, 2017 Dec 1 , 13(45):1701791. https://onlinelibrary.wiley.com/doi/full/10.1002/smll.201701791

5. Deen MJ. Information and communications technologies for elderly ubiquitous healthcare in a smart home. Pers Ubiquitous Comput. 2015 Jul, 19(3):573–99. https://link.springer.com/article/10.1007/s00779-015-0856-x

6. Goodenough JB, Kim Y. Challenges for rechargeable Li batteries. Chem Mater. 2010 Feb 9, 22(3):587–603. https://pubs.acs.org/doi/full/10.1021/cm901452z

7. Chen B, Yang Y, Wang ZL. Scavenging Wind Energy by Triboelectric Nanogenerators. Adv Energy Mater. 2018 Apr 1;8(10):1702649. https://onlinelibrary.wiley.com/doi/full/10.1002/aenm.201702649

8. Tarascon JM, Armand M. Issues and challenges facing rechargeable lithium batteries. Nat 2001 4146861, 2001 Nov 15;414(6861):359–67. https://www.nature.com/articles/35104644

9. Lu L, Yang Z, Meacham K, Cvetkovic C, Corbin EA, Vázquez-Guardado A, et al. Biodegradable Monocrystalline Silicon Photovoltaic Microcells as Power Supplies for Transient Biomedical Implants. Adv Energy Mater, 2018 Jun 1 ;8(16):1703035. https://onlinelibrary.wiley.com/doi/full/10.1002/aenm.201703035

10. Lee DM, Rubab N, Hyun I, Kang W, Kim YJ, Kang M, et al. Ultrasound-mediated triboelectric nanogenerator for powering on-demand transient electronics. Sci Adv, 2022 Jan 1 ;8(1):8423. https://www.science.org/doi/10.1126/sciadv.abl8423

11. Li H, Zhao C, Wang X, Meng J, Zou Y, Noreen S, et al. Fully Bioabsorbable Capacitor as an Energy Storage Unit for Implantable Medical Electronics. Adv Sci, 2019 Mar 1;6(6):1801625. https://onlinelibrary.wiley.com/doi/full/10.1002/advs.201801625

12. Yang Y, Sun N, Wen Z, Cheng P, Zheng H, Shao H, et al. Liquid-Metal-Based Super-Stretchable and Structure-Designable Triboelectric Nanogenerator for Wearable Electronics. ACS Nano, 2018 Feb 27; 12(2):2027–34.

https://pubs.acs.org/doi/full/10.1021/acsnano.8b00147

13. Wang L, Liu W, Yan Z, Wang F, Wang X, Wang L, et al. Stretchable and Shape-Adaptable Triboelectric Nanogenerator Based on Biocompatible Liquid Electrolyte for Biomechanical Energy Harvesting and Wearable Human–Machine Interaction. Adv Funct Mater. 2021 Feb 1;31(7):2007221. https://onlinelibrary.wiley.com/doi/full/10.1002/adfm.202007221

14. Chen X, Parida K, Wang J, Xiong J, Lin MF, Shao J, et al. A Stretchable and Transparent Nanocomposite Nanogenerator for Self-Powered Physiological Monitoring. ACS Appl Mater Interfaces. 2017 Dec 6;9(48):42200–9. https://pubs.acs.org/doi/full/10.1021/acsami.7b13767

15. Shi Q, Zhang Z, Chen T, Lee C. Minimalist and multi-functional human machine interface (HMI) using a flexible wearable triboelectric patch. Nano Energy. 2019 Aug 1;62:355–66.

16. Xia K, Zhu Z, Fu J, Li Y, Chi Y, Zhang H, et al. A triboelectric nanogenerator based on waste tea leaves and packaging bags for powering electronic office supplies and behavior monitoring. Nano Energy. 2019 Jun 1;60:61–71.

17. Ahmed RFSM, Swamy SKK, Chandrasekhar GS, Ankanathappa SM, Chandrasekhar A, Sannathammegowda K. Clitoria ternatea flower extract: Biopolymer composite-based triboelectric nanogenerator as a self-powered smart counter. Surfaces and Interfaces. 2023 Nov 1;42:103369.

18. Begum SR, Chandrasekhar A. Biomimicking hydrophobic leaf structure using soft lithography for fog harvesting, triboelectric nanogenerators as a self-powered rain sensor. iScience. 2024 Feb 16;27(2):108878.

19. Sagade Muktar Ahmed RF, Mohan SB, Madanahalli Ankanathappa S, Shivanna M, Viswanathan P, Manjunatha HCS, et al. Spinach-Mediated Green Synthesized NiFe2O4 Nanoparticle-Based Triboelectric Nanogenerator: A Smart Tollgate Controller. ACS Appl Electron Mater, 2023 Nov 28; 5(11):5885–97. https://pubs.acs.org/doi/full/10.1021/acsaelm.3c00859

20. Luo C, Shao Y, Yu H, Ma H zhi, Zhang Y hao, Gu L, et al. Preparation and application of high performance PVDF/PS electrospinning film-based triboelectric nanogenerator. Chem Phys Lett. 2023 Feb 16;813:140276.

21. Ouyang R, Huang Y, Ye H, Zhang Z, Xue H. Copper particles-PTFE tube based triboelectric nanogenerator for wave energy harvesting. Nano Energy. 2022 Nov 1;102:107749.

22. Singh V, Singh B. MoS2-PVDF/PDMS based flexible hybrid piezo-triboelectric nanogenerator for harvesting mechanical energy. J Alloys Compd. 2023 Apr 25;941:168850.

23. Mao Y, Li Y, Xie J, Liu H, Guo C, Hu W. Triboelectric nanogenerator/supercapacitor in-one self-powered textile based on PTFE yarn wrapped PDMS/MnO2NW hybrid elastomer. Nano Energy. 2021 Jun 1;84:105918.

24. Zhang Z, Cai J. High output triboelectric nanogenerator based on PTFE and cotton for energy harvester and human motion sensor. Curr Appl Phys. 2021 Feb 1;22:1–5.

25. Ahmed AA, Qahtan TF, Afzal N, Rashid M, Thalluri LN, Mohamed Ali MS. Low-pressure air plasma-treated polytetrafluoroethylene surface for efficient triboelectric nanogenerator. Mater Today Sustain. 2023 Mar 1;21:100330.

26. Graham SA, Patnam H, Manchi P, Paranjape MV, Kurakula A, Yu JS. Biocompatible electrospun fibers-based triboelectric nanogenerators for energy harvesting and healthcare monitoring. Nano Energy. 2022 Sep 1;100:107455.

27. Zhao L, Lin Z, Lai KWC. Skin-integrated, stretchable triboelectric nanogenerator for energy harvesting and mechanical sensing. Mater Today Electron. 2022 Oct 1;2:100012.

28. Babu A, Rakesh D, Supraja P, Mishra S, Kumar KU, Kumar RR, et al. Plant-based triboelectric nanogenerator for biomechanical energy harvesting. Results in Surfaces and Interfaces. 2022 Aug 1;8:100075.

29. Qin Y, Zhang W, Liu Y, Zhao J, Yuan J, Chi M, et al. Cellulosic gel-based triboelectric nanogenerators for energy harvesting and emerging applications. Nano Energy. 2023 Feb

1;106:108079.

30. Khandelwal G, Minocha T, Yadav SK, Chandrasekhar A, Maria Joseph Raj NP, Gupta SC, et al. All edible materials derived biocompatible and biodegradable triboelectric nanogenerator. Nano Energy. 2019 Nov 1;65:104016.

31. Kim H, Choi S, Hong Y, Chung J, Choi J, Choi WK, et al. Biocompatible and biodegradable triboelectric nanogenerators based on hyaluronic acid hydrogel film. Appl Mater Today. 2021 Mar 1;22:100920.

32. Sardana S, Singh Z, Sharma AK, Kaur N, Pati PK, Mahajan A. Self-powered biocompatible humidity sensor based on an electrospun anisotropic triboelectric nanogenerator for non-invasive diagnostic applications. Sensors Actuators B Chem. 2022 Nov 15;371:132507.

33. Kim M, Park H, Lee MH, Bae JW, Lee KY, Lee JH, et al. Stretching-insensitive stretchable and biocompatible triboelectric nanogenerators using plasticized PVC gel and graphene electrode for body-integrated touch sensor. Nano Energy. 2023 Mar 1;107:108159.

34. Ma Y, Zheng Q, Liu Y, Shi B, Xue X, Ji W, et al. Self-Powered, One-Stop, and Multifunctional Implantable Triboelectric Active Sensor for Real-Time Biomedical Monitoring. Nano Lett, 2016 Oct 12; 16(10):6042–51. https://pubs.acs.org/doi/full/10.1021/acs.nanolett.6b01968

35. Liu Y, Yu Q, Yang L, Cui Y, Liu Y, Cui Y, et al. Materials and Biomedical Applications of Implantable Electronic Devices. Adv Mater Technol, 2023 Feb 1;8(4):2200853. https://onlinelibrary.wiley.com/doi/full/10.1002/admt.202200853

36. Zheng Q, Zhang H, Shi B, Xue X, Liu Z, Jin Y, et al. In Vivo Self-Powered Wireless Cardiac Monitoring via Implantable Triboelectric Nanogenerator. ACS Nano, 2016 Jul 26;10(7):6510–8. https://pubs.acs.org/doi/full/10.1021/acsnano.6b02693

37. Liu Z, Li H, Shi B, Fan Y, Wang ZL, Li Z. Wearable and Implantable Triboelectric Nanogenerators. Adv Funct Mater, 2019 May 1;29(20):1808820.

https://onlinelibrary.wiley.com/doi/full/10.1002/adfm.201808820

38. Zheng Q, Zou Y, Zhang Y, Liu Z, Shi B, Wang X, et al. Biodegradable triboelectric nanogenerator as a life-time designed implantable power source. Sci Adv, 2016 Mar 1;2(3). https://www.science.org/doi/10.1126/sciadv.1501478

39. Jiang W, Li H, Liu Z, Li Z, Tian J, Shi B, et al. Fully Bioabsorbable Natural-Materials-Based Triboelectric Nanogenerators. Adv Mater, 2018 Aug 1 ;30(32):1801895https://onlinelibrary.wiley.com/doi/full/10.1002/adma.201801895

40. Li Z, Feng H, Zheng Q, Li H, Zhao C, Ouyang H, et al. Photothermally tunable biodegradation of implantable triboelectric nanogenerators for tissue repairing. Nano Energy. 2018 Dec 1;54:390–9.

41. Wang S, Lin L, Wang ZL. Nanoscale triboelectric-effect-enabled energy conversion for sustainably powering portable electronics. Nano Lett, 2012 Dec 12 ;12(12):6339–46. Available from: https://pubs.acs.org/doi/full/10.1021/nl303573d

42. Zhu G, Pan C, Guo W, Chen CY, Zhou Y, Yu R, et al. Triboelectric-generator-driven pulse electrodeposition for micropatterning. Nano Lett, 2012 Sep 12;12(9):4960–5. Available from: https://pubs.acs.org/doi/full/10.1021/nl302560k

43. Khandelwal G, Dahiya R, Khandelwal G, Dahiya R. Self-Powered Active Sensing Based on Triboelectric Generators. Adv Mater, 2022 Aug 1;34(33):2200724. https://onlinelibrary.wiley.com/doi/full/10.1002/adma.202200724

44. Yang Y, Sheng Zhou Y, Zhang H, Liu Y, Lee S, Lin Wang Z, et al. A Single-Electrode Based Triboelectric Nanogenerator as Self-Powered Tracking System. Adv Mater. 2013 Dec 1;25(45):6594–601. https://onlinelibrary.wiley.com/doi/full/10.1002/adma.201302453

45. Wang S, Lin L, Xie Y, Jing Q, Niu S, Wang ZL. Sliding-triboelectric nanogenerators based on in-plane charge-separation mechanism. Nano Lett, 2013 May 8;13(5):2226–33. Available from: https://pubs.acs.org/doi/full/10.1021/nl400738p

46. Zhu G, Chen J, Liu Y, Bai P, Zhou YS, Jing Q, et al. Linear-grating triboelectric generator

based on sliding electrification. Nano Lett [Internet]. 2013 May 8 [cited 2024 Sep 11];13(5):2282–9. Available from: https://pubs.acs.org/doi/full/10.1021/nl4008985

47. Hinchet R, Seung W, Kim SW. Recent Progress on Flexible Triboelectric Nanogenerators for SelfPowered Electronics. ChemSusChem, 2015 Jul 20 ;8(14):2327–44. https://onlinelibrary.wiley.com/doi/full/10.1002/cssc.201403481

48. Wang ZL, Lin L, Chen J, Niu S, Zi Y. Triboelectric Nanogenerator: Lateral Sliding Mode. 2016;49–90. https://link.springer.com/chapter/10.1007/978-3-319-40039-6_3

49. Wang ZL. Triboelectric nanogenerators as new energy technology and self-powered sensors – Principles, problems and perspectives. Faraday Discuss, 2015 Mar 6;176(0):447–58. https://pubs.rsc.org/en/content/articlehtml/2014/fd/c4fd00159a

50. Niu S, Wang S, Lin L, Liu Y, Zhou YS, Hu Y, et al. Theoretical study of contact-mode triboelectric nanogenerators as an effective power source. Energy Environ Sci, 2013 Nov 14;6(12):3576–83. https://pubs.rsc.org/en/content/articlehtml/2013/ee/c3ee42571a

51. Khandelwal G, Deswal S, Dahiya R. Triboelectric Nanogenerators as Power Sources for Chemical Sensors and Biosensors. ACS Omega, 2022 Dec 13;7(49):44573–90. https://pubs.acs.org/doi/full/10.1021/acsomega.2c06335

52. Wu Y, Luo Y, Qu J, Daoud WA, Qi T. Sustainable and shape-adaptable liquid single-electrode triboelectric nanogenerator for biomechanical energy harvesting. Nano Energy. 2020 Sep 1;75:105027.

53. Akram W, Chen Q, Xia G, Fang J. A review of single electrode triboelectric nanogenerators. Nano Energy. 2023 Feb 1;106:108043.

54. Wang S, Xie Y, Niu S, Lin L, Lin Wang Z, Wang S, et al. Freestanding Triboelectric-Layer-Based Nanogenerators for Harvesting Energy from a Moving Object or Human Motion in Contact and Non-contact Modes. Adv Mater, 2014 May 1;26(18):2818–24. https://onlinelibrary.wiley.com/doi/full/10.1002/adma.201305303

55. Wang ZL, Lin L, Chen J, Niu S, Zi Y. Triboelectric Nanogenerator: Freestanding Triboelectric-Layer Mode. Green Energy Technol, 2016;109–53.

https://link.springer.com/chapter/10.1007/978-3-319-40039-6_5

56. Choi D, Lee Y, Lin ZH, Cho S, Kim M, Ao CK, et al. Recent Advances in Triboelectric Nanogenerators: From Technological Progress to Commercial Applications. ACS Nano. 2023 Jun 27;17(12):11087–219. https://pubs.acs.org/doi/full/10.1021/acsnano.2c12458

57. Zhang Y, Zhang T, Huang Z, Yang J. A New Class of Electronic Devices Based on Flexible Porous Substrates. Adv Sci, 2022 Mar 1;9(7):2105084. https://onlinelibrary.wiley.com/doi/full/10.1002/advs.202105084

58. Ghosh SK, Kim MP, Na S, Lee Y, Park J, Cho S, et al. Ultra-stretchable yet tough, healable, and biodegradable triboelectric devices with microstructured and ionically crosslinked biogel. Nano Energy. 2022 Sep 1;100:107438.

59. Bauer S, Kaltenbrunner M. Built to disappear. ACS Nano, 2014 Jun 24 ;8(6):5380–2. https://pubs.acs.org/doi/full/10.1021/nn502938g

60. Zabala A. Illegal electronic waste recycling trends. Nat Sustain, 2019 May 13;2(5):353–4. https://www.nature.com/articles/s41893-019-0289-z

61. Bettinger CJ, Bao Z. Organic Thin-Film Transistors Fabricated on Resorbable Biomaterial Substrates. Adv Mater,. 2010 Feb 2, 22(5):651–5. https://onlinelibrary.wiley.com/doi/full/10.1002/adma.200902322

62. Niu Z, Cheng W, Cao M, Wang D, Wang Q, Han J, et al. Recent advances in cellulose-based flexible triboelectric nanogenerators. Nano Energy. 2021 Sep 1;87:106175.

63. Klemm D, Heublein B, Fink HP, Bohn A. Cellulose: Fascinating Biopolymer and Sustainable Raw Material. Angew Chemie Int Ed, 2005 May 30 ;44(22):3358–93. https://onlinelibrary.wiley.com/doi/full/10.1002/anie.200460587

64. Ling S, Chen W, Fan Y, Zheng K, Jin K, Yu H, et al. Biopolymer nanofibrils: Structure, modeling, preparation, and applications. Prog Polym Sci. 2018 Oct 1;85:1–56.

65. Klemm D, Kramer F, Moritz S, Lindström T, Ankerfors M, Gray D, et al. Nanocelluloses: A New Family of Nature-Based Materials. Angew Chemie Int Ed. 2011 Jun

6;50(24):5438–66. https://onlinelibrary.wiley.com/doi/full/10.1002/anie.201001273

66. Moon RJ, Martini A, Nairn J, Simonsen J, Youngblood J. Cellulose nanomaterials review: structure, properties and nanocomposites. Chem Soc Rev. 2011 Jun 20;40(7):3941–94. https://pubs.rsc.org/en/content/articlehtml/2011/cs/c0cs00108b

67. Lamanna L, Pace G, Ilic IK, Cataldi P, Viola F, Friuli M, et al. Edible cellulose-based conductive composites for triboelectric nanogenerators and supercapacitors. Nano Energy. 2023 Apr 1;108:108168.

68. Chen Y, Li D, Xu Y, Ling Z, Nawaz H, Chen S, et al. Surface-microstructured cellulose films toward sensitive pressure sensors and efficient triboelectric nanogenerators. Int J Biol Macromol. 2022 May 31;208:324–32.

69. Chen S, Jiang J, Xu F, Gong S. Crepe cellulose paper and nitrocellulose membrane-based triboelectric nanogenerators for energy harvesting and self-powered human-machine interaction. Nano Energy. 2019 Jul 1;61:69–77.

70. Kim HJ, Yim EC, Kim JH, Kim SJ, Park JY, Oh IK. Bacterial Nano-Cellulose Triboelectric Nanogenerator. Nano Energy. 2017 Mar 1;33:130–7.

71. Karim AA, Bhat R. Fish gelatin: properties, challenges, and prospects as an alternative to mammalian gelatins. Food Hydrocoll. 2009 May 1;23(3):563–76.

72. Yoshimura K, Terashima M, Hozan D, Ebato T, Nomura Y, Ishii Y, et al. Physical properties of shark gelatin compared with pig gelatin. J Agric Food Chem. 2000 Jun;48(6):2023–7. https://pubs.acs.org/doi/full/10.1021/jf990887m

73. Olatunji O, Olubowale M, Okereke C. Microneedle-assisted transdermal delivery of acetylsalicylic acid (aspirin) from biopolymer films extracted from fish scales. Polym Bull. 2018 Sep 1;75(9):4103–15. https://link.springer.com/article/10.1007/s00289-017-2254-1

74. Yoon H-J, Lee D-M, Kim Y-J, Jeon S, Jung J-H, Soo Kwak S, et al. Mechanoreceptor-Inspired Dynamic Mechanical Stimuli Perception based on Switchable Ionic Polarization. Adv Funct Mater. 2021 Jun 1;31(23):2100649.

https://onlinelibrary.wiley.com/doi/full/10.1002/adfm.202100649

75. Wu M, Wang X, Xia Y, Zhu Y, Zhu S, Jia C, et al. Stretchable freezing-tolerant triboelectric nanogenerator and strain sensor based on transparent, long-term stable, and highly conductive gelatin-based organohydrogel. Nano Energy. 2022 May 1;95:106967.

76. Han Y, Han Y, Zhang X, Li L, Zhang C, Liu J, et al. Fish Gelatin Based Triboelectric Nanogenerator for Harvesting Biomechanical Energy and Self-Powered Sensing of Human Physiological Signals. ACS Appl Mater Interfaces. 2020 Apr 8;12(14):16442–50. https://pubs.acs.org/doi/full/10.1021/acsami.0c01061

77. Ma C, Gao S, Gao X, Wu M, Wang R, Wang Y, et al. Chitosan biopolymer-derived self-powered triboelectric sensor with optimized performance through molecular surface engineering and data-driven learning. InfoMat. 2019 Mar 1;1(1):116–25. Available from: https://onlinelibrary.wiley.com/doi/full/10.1002/inf2.12008

78. Charoonsuk T, Supansomboon S, Pakawanit P, Vittayakorn W, Pongampai S, Woramongkolchai S, et al. Simple enhanced charge density of chitosan film by the embedded ion method for the flexible triboelectric nanogenerator. Carbohydr Polym. 2022 Dec 1;297:120070.

79. Rebello S, Sali S, Jisha MS, Reshmy R, Pugazhendhi A, Madhavan A, et al. Chitosan a versatile adsorbent in environmental remediation in the era of circular economy-a mini review. Sustain Chem Pharm. 2023 May 1;32:101004.

80. Charoonsuk T, Pongampai S, Pakawanit P, Vittayakorn N. Achieving a highly efficient chitosan-based triboelectric nanogenerator via adding organic proteins: Influence of morphology and molecular structure. Nano Energy. 2021 Nov 1;89:106430.

81. Kim JN, Lee J, Go TW, Rajabi-Abhari A, Mahato M, Park JY, et al. Skin-attachable and biofriendly chitosan-diatom triboelectric nanogenerator. Nano Energy. 2020 Sep 1;75:104904.

82. Kim JN, Lee J, Lee H, Oh IK. Stretchable and self-healable catechol-chitosan-diatom hydrogel for triboelectric generator and self-powered tremor sensor targeting at Parkinson

disease. Nano Energy. 2021 Apr 1;82:105705.

83. Jiang C, Wu C, Li X, Yao Y, Lan L, Zhao F, et al. All-electrospun flexible triboelectric nanogenerator based on metallic MXene nanosheets. Nano Energy. 2019 May 1;59:268–76.

84. Zhang XS, Brugger J, Kim B. A silk-fibroin-based transparent triboelectric generator suitable for autonomous sensor network. Nano Energy. 2016 Feb 1;20:37–47.

85. Candido ICM, Oliveira G da S, Ribeiro SJL, Cavicchioli M, Barud HS, Silva LG, et al. PVA-silk fibroin bio-based triboelectric nanogenerator. Nano Energy. 2023 Jan 1;105:108035.

86. Niu Q, Huang L, Lv S, Shao H, Fan S, Zhang Y. Pulse-driven bio-triboelectric nanogenerator based on silk nanoribbons. Nano Energy. 2020 Aug 1;74:104837.

87. Yao G, Kang L, Li J, Long Y, Wei H, Ferreira CA, et al. Effective weight control via an implanted self-powered vagus nerve stimulation device. Nat Commun 2018 91. 2018 Dec 17 ;9(1):1–10. https://www.nature.com/articles/s41467-018-07764-z

88. Wang C, Shi Q, Lee C. Advanced Implantable Biomedical Devices Enabled by Triboelectric Nanogenerators. Nanomater 2022, Vol 12, Page 1366. 2022 Apr 15 ;12(8):1366. https://www.mdpi.com/2079-4991/12/8/1366/htm

89. Li J, Kang L, Long Y, Wei H, Yu Y, Wang Y, et al. Implanted Battery-Free Direct-Current Micro-Power Supply from in Vivo Breath Energy Harvesting. ACS Appl Mater Interfaces. 2018 Dec 12;10(49):42030–8. https://pubs.acs.org/doi/full/10.1021/acsami.8b15619

90. Gélat P, Ter Haar G, Saffari N. The optimization of acoustic fields for ablative therapies of tumours in the upper abdomen. Phys Med Biol. 2012 Dec 4;57(24):8471. https://iopscience.iop.org/article/10.1088/0031-9155/57/24/8471.

91. Seo D, Neely RM, Shen K, Singhal U, Alon E, Rabaey JM, et al. Wireless Recording in the Peripheral Nervous System with Ultrasonic Neural Dust. Neuron. 2016 Aug 3;91(3):529–39.

92. Jiang L, Yang Y, Chen Y, Zhou Q. Ultrasound-induced wireless energy harvesting: From materials strategies to functional applications. Nano Energy. 2020 Nov 1;77:105131.

93. Imani IM, Kim B, Xiao X, Rubab N, Park BJ, Kim YJ, et al. Ultrasound-Driven On-Demand Transient Triboelectric Nanogenerator for Subcutaneous Antibacterial Activity. Adv Sci, 2023 Jan 1;10(3):2204801. https://onlinelibrary.wiley.com/doi/full/10.1002/advs.202204801

94. Meng X, Xiao X, Jeon S, Kim D, Park B-J, Kim Y-J, et al. An Ultrasound-Driven Bioadhesive Triboelectric Nanogenerator for Instant Wound Sealing and Electrically Accelerated Healing in Emergencies. Adv Mater. 2023 Mar 1;35(12):2209054. https://onlinelibrary.wiley.com/doi/full/10.1002/adma.202209054

95. Deng W, Libanori A, Xiao X, Fang J, Zhao X, Zhou Y, et al. Computational investigation of ultrasound induced electricity generation via a triboelectric nanogenerator. Nano Energy. 2022 Jan 1;91:106656.

96. Pavlov VA, Tracey KJ. The vagus nerve and the inflammatory reflex—linking immunity and metabolism. Nat Rev Endocrinol. 2012 Nov 21;8(12):743–54. https://www.nature.com/articles/nrendo.2012.189

97. Groves DA, Brown VJ. Vagal nerve stimulation: a review of its applications and potential mechanisms that mediate its clinical effects. Neurosci Biobehav Rev. 2005 May 1;29(3):493–500.

98. Borovikova L V., Ivanova S, Zhang M, Yang H, Botchkina GI, Watkins LR, et al. Vagus nerve stimulation attenuates the systemic inflammatory response to endotoxin. Nat 2000 4056785 [Internet]. 2000 May 25 [cited 2024 Sep 11];405(6785):458–62. Available from: https://www.nature.com/articles/35013070

99. Chen P, Wang Q, Wan X, Yang M, Liu C, Xu C, et al. Wireless electrical stimulation of the vagus nerves by ultrasound-responsive programmable hydrogel nanogenerators for anti-inflammatory therapy in sepsis. Nano Energy. 2021 Nov 1;89:106327.

100. Lee S, Wang H, Shi Q, Dhakar L, Wang J, Thakor N V., et al. Development of battery-free neural interface and modulated control of tibialis anterior muscle via common peroneal nerve based on triboelectric nanogenerators (TENGs). Nano Energy. 2017 Mar 1;33:1–11.

Data Availability Statement

Data will be available if there is any request from reviewers or Editors